Author Manuscript

Author Manuscript

Author Manuscript

Author Manuscript

HHS Public Access

Author manuscript

Bone. Author manuscript; available in PMC 2016 October 01.

Published in final edited form as:

Bone. 2015 October ; 79: 131–142. doi:10.1016/j.bone.2015.05.030.

Age dependent regulation of bone-mass and renal function by the MEPE ASARM-motif

Lesya V Zelenchuk, **Anne-Marie Hedge**, and **Peter S N Rowe**

The Kidney Institute, Kansas University Medical Center, Kansas City KS, USA.

Abstract

Context—Mice with null mutations in Matrix Extracellular Phosphoglycoprotein (MEPE) have increased bone mass, increased trabecular density and abnormal cancellous bone (MN-mice). These defects worsen with age and MEPE over expression induces opposite effects. Also, Genome Wide Association studies show MEPE plays a major role in bone mass. We hypothesized the conserved C-terminal MEPE ASARM-motif is chiefly responsible for regulating bone mass and trabecular structure.

Design—To test our theory we over expressed C-terminal ASARM-peptide in MN-mice using the Col1α1 promoter (MNAt-mice). We then compared the bone and renal phenotypes of the MNAt-mouse with the MN-mouse and the X-linked hypophosphatemic rickets mouse (HYP). The HYP mouse over expresses ASARM-peptides and is defective for the PHEX gene.

Results—The MN-mouse developed increased bone mass, bone strength and trabecular abnormalities that worsened markedly with age. Defects in bone formation were chiefly responsible with suppressed sclerostin and increased active β-catenin. Increased uric acid levels also suggested abnormalities in purine-metabolism and a reduced fractional excretion of uric acid signaled additional renal transport changes. The MN mouse developed a worsening hyperphosphatemia and reduced FGF23 with age. An increase in the fractional excretion of phosphate (FEP) despite the hyperphosphatemia confirms an imbalance in kidney-intestinal phosphate regulation. Also, the MN mice showed an increased creatinine clearance suggesting hyperfiltration. A reversal of the MN bone-renal phenotype changes occurred with the MNAt mice including the apparent hyperfiltration. The MNAt mice also developed localized hypomineralization, hypophosphatemia and increased FGF23.

Conclusions—The C-terminal ASARM-motif plays a major role in regulating bone–mass and cancellous structure as mice age. In healthy mice, the processing and release of free ASARM-

Address all correspondence to: Peter S N Rowe, Department of Internal Medicine, Division of Nephrology and Hypertension, The Kidney Institute, MS 3018, 3901 Rainbow Boulevard, Kansas City, KS 66160 USA, Tel: 913 588 0704 Fax: 913 588 9252 prowe@kumc.edu.

Publisher's Disclaimer: This is a PDF file of an unedited manuscript that has been accepted for publication. As a service to our customers we are providing this early version of the manuscript. The manuscript will undergo copyediting, typesetting, and review of the resulting proof before it is published in its final citable form. Please note that during the production process errors may be discovered which could affect the content, and all legal disclaimers that apply to the journal pertain.

Disclosure statement: Authors (LZ, AM and PR) have nothing to disclose.

Supplemental data

Supplemental data include supplemental legends, two figures (Figures S1 and S2) and two tables (Tables S1 and S2). In the text, supplemental figure and table numbers are prefixed with the letter S.

Author Manuscript Author Manuscript Author Manuscript Author Manuscript

peptide is chiefly responsible for preserving normal bone and renal function. Free ASARM-peptide also effects renal mineral phosphate handling by influencing FGF23 expression. These findings have implications for understanding age-dependent osteoporosis, unraveling drug-targets and developing treatments.

Keywords

Rickets; Mineralization; MEPE; DMP1; FGF23; PHEX; Hypophosphatemia; PTH; Vitamin D; Sclerostin; X-linked hypophosphatemic rickets; HYP; XLH; bone quality; renal phosphate regulation; ASARM-peptide; SIBLING proteins

Introduction

Osteoporosis and a decline in estimated glomerular filtration rate (eGFR) occur in elderly patients and are major global health issues (1,2). Understanding the underlying disease process and etiology is important for developing drugs, early screening measures and preventive strategies. Compelling evidence exists for the role of Matrix-*E*xtracellular-Phospho-GlycoprotEin with ASARM-motif (MEPE), an osteocyte and kidney expressed protein (3,4). MEPE regulates bone-mass (3,5-18) and genome wide association studies (GWA) confirm MEPE is a major gene locus for bone mineral density (BMD) and osteoporosis (19-26). Serum phosphorus, parathyroid hormone and bone BMD correlate significantly with circulating MEPE protein (9,27). Bone mass and trabecular content increase as MEPE null-mice age and decrease in mice over expressing MEPE (14,18). MEPE contains a conserved C-terminal region known as the ASARM-motif that occurs in a family of proteins called Short Integrin Binding Ligand Interacting Glycoproteins (SIBLINGs) (28). These include DMP1, OPN, DSPP, Statherin and BSP that all map to chromosome 4 in mice and 5 in humans. DMP1 is the closest family member to MEPE and loss of DMP1 results in autosomal recessive hypophosphatemic rickets (ARHR-I). The released ASARM-motif or ASARM-peptide and full length MEPE protein inhibit renal and intestinal phosphate uptake and bone mineralization (7,8,11,14-17,29-34). SIBLING proteins MEPE and DMP1 interact with PHEX and influence FGF23 expression. Bone-derived ASARM-peptides modulate these interactions and thereby regulate mineralization, bone turnover and phosphate. Indeed, ASARM-peptides are the only known physiological substrate for PHEX (15-17,29,30,35,36). Compelling evidence shows the ratio of ASARM-peptide to SIBLING-protein plays a role in regulating the mineral matrix and FGF23 production. This in turn moderates systemic phosphate and vitamin-D metabolism (8,14,16,31,32,37). Also, our work has now provided compelling evidence that ASARM-peptides are responsible for the mineralization defect and component to the hypophosphatemia in HYP and ARHR (4-7,9-17,29,30,35,38,39).

The high degree of conservation of the MEPE ASARM-motif prompted us to study its role in mediating the bone-renal functions of MEPE. To do this we over expressed C-terminal ASARM-peptide in MN-mice by using the Col1α1 promoter (MNAt-mice). We then compared the bone and renal phenotypes of the MNAt-mouse with the MN-mouse and the X-linked hypophosphatemic rickets mouse (HYP). The HYP mouse over expresses ASARM-peptides and is defective for the PHEX gene. Our study shows the C-terminal

Author Manuscript Author Manuscript Author Manuscript Author Manuscript

ASARM-motif plays a major role in regulating bone–mass and cancellous structure as mice age. In healthy mice, processing and release of free ASARM-peptide is chiefly responsible. Free ASARM-peptide also effects renal mineral phosphate handling by influencing FGF23 expression and the N-terminal part of MEPE may influence purine metabolism and uric acid (UA) production. These findings have implications for understanding age-dependent osteoporosis, unraveling drug-targets and developing treatments.

Materials and Methods

Animals, serum and urine collection

The murine MEPE$^{-/-}$ mice (MN) used in this study have been described and are a C57BL/6 strain (18). A transgenic C57BL/6 mouse model expressing murine ASARM-peptide with signal-peptide and short linker region under the control of a Col1α1 2.3 kb promoter (At-mice) was prepared using pronuclear microinjection (Figure 1, Figure S1 and Figure S2). The cloning vector (pJ251) was previously reported (14,40) and the map/sequence of the construct is detailed in Figure 1A, Figure S1 and Figure S2. The signal peptide and short linker peptide were added to ensure processing and extracellular release of ASARM-peptide (Figure S1). The complete sequence of the ASARM-peptide transgenic (At-mice) construct is provided in supplementary Figure S2. The MN and At-mice were then mated to generate a combined MEPE$^{-/-}$/ASARM-peptide transgenic (MNAt-mice). Figure 1A depicts the transgene construct with primers used to screen the mice and Figure 1B and C show typical PCR and southern blot screens for MN, MNAt and WT mice. The primers used are described below and in the legends of Figure 1 and also highlighted in the complete sequence shown in Figure S2. ASARM-peptide expression was confirmed by an ASARM-ELISA and by immunohistology as reported previously (9,11,14-16,33,34,41). Male mice fed 1% PO4/2.4IU/g vitamin D (Harlan Teklad 8604) diet and at least six animals per experimental group were studied over an 8 month period. Beginning at 6 weeks of age, blood samples were collected every week by tail bleed as described in the results section for the duration of the experiment (16 weeks). Prior to termination, mice (22 weeks of age) were housed overnight in metabolic cages with water but without food as described previously (8,11,14,16,33,34). Urine was then collected and blood removed (under anesthesia) by intracardiac exsanguination. Specifically an intraperitoneal (ip) overdose of 120 μg/g of ketamine and 80 μg/g xylazine solutions (*Phoenix Pharmaceutical Inc., MO; USA*) was given as anesthetic prior to cardiac exsanguination. Animal care and protocols were in accordance with institutional guidelines of the university of Kansas Medical Center (KUMC) as detailed in the Guide for the Care and Use of Laboratory Animals prepared by the Institute on Laboratory Animal Resources, National Research Council (DHHS Publ. NIH 86-23, 1985).

Genotyping by southern and PCR

For genotyping the MEPE$^{+/+}$/ASARM transgenic mice (**At-mice**) by PCR, a 2891-bp product was amplified using primers GX2192: 5’-CTT GGA ACC CAT TGC CTT CAA CTCC-3’and GX2193: 5’-CAC GCA GGA GTT TTG ATG GAC TTGC-3’ to amplify a 2891 bp band (PCR, 35 cycles annealing 65C; Figure 1A, B and Figure S2). For secondary confirmation by southern blot, primers mep2199: 5’-GTT CCT AAG CAG ATT GGA CAG

Author Manuscript Author Manuscript Author Manuscript Author Manuscript

AGC ACC-3' and mep2200: 5'-AGT TTG TTG CAG GAA GCC TGT GACC -3' were used to amplify vector cloned transgene to generate a 458 bp fragment (PCR, 35 cycles annealing 65C). This fragment was then used to screen genomic blots of BgII and BamHI restriction digested genomic DNA to yield an 1891 bp transgenic band (Figures 1C and S2). The complete sequence of the vector cloned construct with highlighted primer positions is shown in Figure S2. For genotyping previously reported MEPE$^{-/-}$ (**MN-mice**) (18), the following primers were used to amplify the neo cassette to generate a 430 bp band: NEO50F 5'-AGA GGC TAT TCG GCT ATG ACT G-3' and NEO430R: 5'-TTC GTC CAG ATC ATC CTG ATC-3' (Figure 1B). Finally, to genotype wild-type **MEPE**$^{+/+}$ by PCR, a 215 bp band was amplified using primers MEPEWTF: 5'-CCG CTG TGA CAT CCC TTT AT-3' and MEPEWTR: 5'- CCC AAG AGC AGC AAA GGT AG-3' (Figure 1B). Figure 1A, B and C illustrates the map, PCR data and southern results. For genotyping the **MNAt-mice** (MEPE$^{-/-}$/ASARM-transgenic), we used a combination of **At** mice primer and southern and **MN** primers as illustrated in Figure 1. Also, Figure S1 shows the ASARM construct with linker, spacer and a 3D representation of the transgenic ASARM-peptide. The complete sequence and highlighted primers for the ASARM-transgenic cloning vehicle is shown in Figure S2.

Serum and Urine Analysis

At specific intervals throughout the experiment as detailed in the results, tail blood-samples were collected in serum-separator tubes and serum prepared as described previously (8,11,14,33,34). On the final day of the experiment (day 112 (16 weeks); mice were 22 weeks old) blood and urine were collected from mice fasted overnight in metabolic cages with full access to water (1 cage/mouse). The blood from the final bleeds were collected by cardiac exsanguination and serum urinalysis carried out as described previously (8,11,14,16,17,33,34). Briefly, Osteocalcin (Mouse Osteocalcin EIA Kit; BTI, Stoughton, MA), alkaline phosphatase (Liquid Alkaline Phosphatase; Pointe Scientific Inc., Canton, MI), $1,25(OH)_2D_3$ (IDS Inc., Fountain Hills, AZ) and FGF23 (Kainos Laboratories Inc., Tokyo, Japan) were measured on serum samples. Inorganic phosphorus, calcium, creatinine (Pointe Scientific Inc, Canton, MI), Osteopontin (Quantikine Mouse Osteopontin; R&D Systems, Minneapolis, MN) and MEPE protein levels (MyBioSource.com; San Diego CA, USA) were assessed both in serum and urine. A competitive ELISA kit was used for the ASARM-peptide measurement as previously published for serum and urine samples (9,11,14,33,34).

Bone Analysis: micro computed tomography (μCT) & Dual X-Ray Absorptiometry (DEXA)

Dual X-Ray Absorptiometry (DEXA) using a PIXImus system (LUNAR Corporation, Madison, WI) and micro computed tomography (μCT) using a Scanco μCT 40 system was carried out as described previously (14,16,33,34). Mice bones and kidneys (fixed and ethanol dehydrated) were scanned with a high-resolution μCT (μCT40; Scanco Medical, Southeastern, PA) as previously described (14,16,33). Data were acquired at 55 KeV and 6 μm cubic resolutions for isolated specimens. Three-dimensional reconstructions for bone samples were generated with the following parameters: Sigma, 0.8; Support, 1; Threshold, 250 (spongiosa) or 280 (cortex). Cortical thickness and tissue mineral density were calculated by integration of the value on each transverse section of a set of 150 chosen in the

Author Manuscript Author Manuscript Author Manuscript Author Manuscript

midshaft area. Tissue mineral density was derived from the linear attenuation coefficient of thresholded bone through precalibration of the apparatus for the acquisition voltage chosen. The bone volume fraction of trabecular metaphysis (VOX BV/TV) was measured on a set of 100 sections under the growth plate, within the secondary spongiosa. Trabecular thickness (Tb.Th), trabecular number (Tb.N), trabecular separation (Tb.Sp), and structure model index (SMI) were calculated without assuming a constant model, as previously described (14,16,33). SMI estimates the plate-rod characteristics of a structure; its value is 0 for an ideal plate, and 3 for an ideal rod, with intermediate values reflecting the volume ratio between rods and plates. For the assessment of bone microstructure in rodents the guidelines detailed by Bouxsein et al 2010 (42) and standardized as described by Parfitt et al 1987 (43). A dual energy X-ray PIXImus densitometer (LUNAR Corporation, Madison, WI) was used for measuring bone mineral density (BMD). Four different sites were determined by adjusting the region of interest (ROI): entire humerus, entire femur, entire tibia and L1 to L5 vertebrae. ROI was adjusted on each bone length and width.

Bone Histology and Histomorphometry

Bone histology histomorphometry was carried out as described previously (14,16,33,34). Specifically, bone growth was assessed by slide caliper measurement of bone length. Animals were labeled by intraperitoneal (ip) injection of 30 μg/g tetracycline, 40 μg/g alizarin complexone-dehydrate and 15 μg/g calcein (Sigma-Aldrich Co, MO, USA) respectively on day 9, 6 and 3 prior to sacrifice. Bones were excised, fixed, dehydrated in ethanol, and embedded in methylmethacrylate at low temperature. Longitudinal coronal slices were cut with a Leica model RM2255 microtome (Leica Biosystems; Buffalo Grove, IL USA 60089) and used for modified Goldner staining, tartrate-resistant acid phosphatase (TRAcP), alkaline phosphatase (ALP) or left unstained. Trabecular bone volume (BV/TV), osteoid surface (OS/BS), osteoid thickness (O.Th) and osteoid volume (OV/BV) were measured on Goldner sections. Dynamic bone remodeling parameters were measured by histomorphometry on unstained sections for mineral-surface/bone-surface (MS/BS), mineral apposition rate (MAR), and BFR (BFR/BS). These parameters were combined to assess osteoid mineralization through MLT (MLT = [O.Th × OS]/[MS × MAR]) and Osteoid Maturation Time (OMT = O.Th/MAR). Osteoclast surfaces (Oc.S/BS) and numbers (N.Oc/B.Ar; N.Oc/BPm) were measured on tartrate resistant acid phosphatase (TRAcP) stained sections. Widths of proliferative and hypertrophic chondrocytes zones were measured at multiple sites along the growth plate. Non-decalcified histology following tetracycline labeling was used to assess bone histologically. Explora-Nova histomorphometric software (F17011 LA Rochelle Cedex 1 France) was used to analyze the microscopically imaged samples and the guidelines described by Ott 2008 (44) were used to calculate histomorphometric measurements of bone turnover, mineralization and volume. Bone histomorphometric nomenclature, symbols and units were standardized as described by Parfitt et al 1987 (43).

RNA Isolation, tissue extraction, Real Time PCR analysis & Western Blotting analysis

The above methods were performed as described previously (11,14,15,33,34) with specific polyclonal primary antibodies and primers shown in Tables S1 and S2 respectively. Transferrin was used as an internal reference for all protocols (RNA and protein) since our

Author Manuscript Author Manuscript Author Manuscript Author Manuscript

previous studies showed GAPDH is markedly suppressed in HYP-mice bone (−× 6.2) and kidney (−× 2.0) (33,34). The Pfaffl mathematical model for the relative quantification of real-time PCR data was used to measure relative gene expression (45). For gene analysis mRNA was prepared from whole kidneys or femurs that were snap frozen in liquid nitrogen and homogenized. For qRT-PCR gene analysis fold differences in expression calculated by the Pfaffl method (45) were statistically analyzed for significance using the *One Sample t-test* and the *Wilcoxon Signed rank-test* with *theoretical means set to 1* as reported previously (11,14,15,33,34). For each primer set the PCR efficiency (E) was calculated and the Pfaffl equation was used to measure expression of each respective gene (45). Individual samples from each mouse were measured in triplicate and experiments repeated three times using 96 well plates with *all phenotype combinations*. A minimum of 6 mice were used for each group. The four groups were then compared using one way analysis of variance *(ANOVA) followed by Tukey multi-comparison*.

Immunohistochemistry (IHC)

Immunohistochemistry was carried out as described previously (14-16,33,34). Specifically, proximal tibias and distal femurs were decalcified in 0.1M EDTA aqueous solution for 2 weeks until complete demineralization. Decalcified bones and left kidneys were dehydrated in absolute ethanol and embedded in paraffin. 5 m thick sections were cut on a rotary microtome. Sections were dried overnight on pre-charged pre-cleaned slides (VWR Scientific, PA., USA), deparaffinized and rehydrated. Osteoblastic and osteoclastic cell cultures were cultured as described previously on BD cell-culture treated bio slides and processed in the same manner as tissue sections (14,15). For immunohistochemistry, after antigen retrieval by incubation in citric acid buffer 10mM pH 3 for 60min at 37°C, nonspecific sites were blocked with 1X animal free blocker (Vector Laboratories Inc., CA, USA) and then sections were incubated with specific primary antibodies for 1 hour. An immunohistological vectastain ABC kit (Vector Laboratories Inc., CA, USA) is routinely used and slides counterstained with DAPI or methyl-green, dehydrated and mounted with entellan. Polyclonal primary antibodies used are detailed in supplementary Table S1.

Statistical analyses

Statistical analysis was performed using statistical software STATISTICA (StatSoft Inc., Tulsa, OK, USA) or PRISM5 (GraphPad Software inc., La Jolla, CA USA). Differences between groups were initially analyzed by two-way ANOVA. When F values for a given variable were found to be significant, the sequentially rejecting Bonferroni-Holm test was subsequently performed using the Holm's adjusted p values. For qRT-PCR gene analysis fold differences in expression calculated by the Pfaffl method(45) were statistically analyzed for significance using the One Sample t-test and the Wilcoxon Signed rank-test with theoretical means set to 1. Results for all tests were considered to be significantly different at $p<0.05$.

Author Manuscript Author Manuscript Author Manuscript Author Manuscript

Results

Generation of the MEPEtg$^{-/-}$/ASARM transgene (MNAt) mouse model

MN mice lacked circulating MEPE protein (Table 1) and stained negatively for MEPE expression in bone (not shown), with no detectable MEPE mRNA expression in bone and kidney (Tables 2 & 3). Although markedly decreased, measurable circulating ASARM-peptides still occurred in MN mice (Table 1). These residual ASARM-peptides were likely derived from other SIBLINGs like DMP1, osteopontin and DSPP. MNAt mice also lacked MEPE expression but over expressed ASARM-peptides in bone and serum (Table 1). Of note, the ELISA used for whole MEPE measurements did not detect free ASARM-peptide (data not shown). As reported previously, increased expression and protein levels of MEPE and ASARM-peptides occurred in circulation, urine, bone and kidneys of HYP mice (Table 1 and Table 2) (9,11,16,33,34,41). Intercrosses between MN and At mice, revealed a normal Mendelian frequency for MNAt (50% expected). Survival rate from birth to weaning (90%) was identical to wild type littermates. Despite a normal appearance, body weight was significantly reduced suggesting abnormal growth (−80%). No differences in food intake between wild type (WT), MN, At or MNAt mice were noted (data not shown). Renal blood urea nitrogen (BUN) levels and urine protein were also normal for all mice. Circulating ASARM-peptide levels correlated positively with ASARM-transgenic copy number (r^2=0.8636 and p(two tailed)=0.0073; 95% confidence interval 0.4789 to 0.9924, Pearson correlation test; data not shown).

MEPE and ASARM-peptides are age-dependent regulators of serum phosphorus & FGF23

Both HYP mice and MNAt mice shared the high circulating ASARM-peptide levels, hypophosphatemia, increased FGF23, PTH and alkaline phosphatase relative to WT mice (Tables 1, 3 & 4; Figure 2 and Figure 3). Also, a reduction in 1,25$(OH)_2$ D_3 occurred with MNAt mice that persisted overtime and mirrored a decreased renal expression of 1 α-hydroxylase (CYP27B1) but not 24-Hydroxylase (CYP24A1); anabolic and catabolic enzymes of vitamin-D metabolism respectively (Figure 3C and Table 3). As reported previously by several groups including ours, HYP-mice displayed inappropriately normal serum 1,25$(OH)_2D_3$ despite increased renal expression of 1 α-hydroxylase (33,34,46-48). Consistent with these hormonal changes, MNAt mice and HYP mice showed increased fractional excretions of phosphate (FEP) with hypophosphatemia (Tables 1 & 4). This accompanied a decreased renal expression of the Na^+-dependent phosphate cotransporters NAPT2a (slc34a1) and NPT2c (slc34a3) (Figure 2 and Table 3). Note, for NPT2A both renal-expression (mRNA) and protein were measured and shown to be reduced (Table 3 and Figure 2). For NPT2C only renal mRNA expression was measured (Table 3).

In contrast to MNAt and HYP mice, MN mice displayed reduced FGF23 and no significant changes in PTH or alkaline phosphatase (Table 1 and Table 2). Also, in direct contrast to MNAt mice, increased serum 1,25$(OH)_2$ D_3 levels with increased renal Na^+-dependent phosphate co-transporter expression occurred with MN mice. The increases included both the NPT2a (slc34a1; protein and mRNA) and NPT2c (slc34a3; mRNA) phosphate-transporters (Figures 2(A & B), 3(A & B), Table 1 and Table 3). This resulted in hyperphosphatemia suggesting a role for intact MEPE protein in preserving long-term

Author Manuscript Author Manuscript Author Manuscript Author Manuscript

phosphate homeostasis. Specifically, the hyperphosphatemia worsened progressively as the MN-mice aged; young MN-mice remained normophosphatemic (Figure 3(A & B)). Remarkably and unexpectedly, despite the hyperphosphatemia (Table 1 and Figure 3(A & B)) increased NPT2ac kidney expression (Figure 2(A & B) and Table 3), mature MN mice displayed an increased urinary FEP (Table 4). All the mutant mice studied (MN, MNat and HYP mice) remained normacalcemic (Table 1). Despite normacalcemia, MN mice showed a reduced fractional excretion of calcium consistent with the increased serum $1,25(OH)_2$ and renal 1-α-hydroxylase expression (Figures 3C and Tables 1, 3 & 4). Also, in contrast to the other mice with normal creatinine clearance, an increased creatinine clearance occurred with MN mice pointing to a possible renal hyperfiltration abnormality (Table 4). Intriguingly, the MN mice also showed increased expression of renal VEGF (Table 3). The increased VEGF expression is consistent with the MN mice hyperfiltration hypothesis. This is because of the inferred VEGF altered vascular supply and thus renal plasma blood flow. Consistent with this interpretation, we previously reported altered renal vasculogenesis in transgenic mice over expressing full-length MEPE (14). Of note, the MN mice maintained normal fasting glucose levels suggesting the "*apparent*" hyperfiltration was not because of incipient diabetes. Importantly, although creatinine clearance is one of the most common methods used to estimate GFR we cannot discount the possibility that an increased renal secretion of creatinine is responsible and not GFR. Specifically, in C57BL/6 mice there is a significant secretory contribution to creatinine excretion mediated through the organic anion transport system (49). Thus, further studies are needed to confirm whether MN mice show a hyperfiltration abnormality or an increased renal excretion of creatinine.

N-terminal MEPE regulates serum uric acid (UA) levels and renal handling of UA

Both MN and MNAt mice exhibited significant hyperuricemia and reduced fractional excretion of uric acid (UA) (Tables 1 and 4). Since both mice lacked the N-terminal portion of MEPE this suggests a role for this region in regulating uric acid metabolism. Consistent with this interpretation, HYP mice over expressing MEPE showed an opposite hypouricemia and increased fractional excretion of UA. Intriguingly, as discussed earlier, although both MNAt and HYP mice exhibited hypophosphatemia MN mice displayed hyperphosphatemia confounding a link with serum phosphate, uric acid and purine metabolism. Also, previous human studies show high levels of uric acid are associated positively with bone mass (50-52).

ASARM over expression corrects MN-mice bone mass & trabecular bone defects

Our studies agree with previous reports that showed MN mice have increased bone mass with increased trabecular number and content (18). Both histological and μCt tomographic analyses showed major increases in trabecular number (Tb.N), thickness (Tb.Th) and bone volume/tissue volume (BV/TV) (Figure 4; Tables 5 and 6). These changes are primarily associated with increased bone formation and not by altered bone resorption. Specifically, an increased mineral apposition rate (MAR), bone formation rate (BFR/TV), and osteoblast numbers occurred with MN mice (Table 5). For the first time we showed using high resolution μCT analysis the MN mouse epiphyseal cortical ring thickness is reduced and the BV/TV of the epiphyseal ring is unchanged. The moment of inertia index (MOI) of this ring and thus inferred bone strength is significantly increased. In contrast, a major increase in the

Author Manuscript Author Manuscript Author Manuscript Author Manuscript

BV/TV of the trabecular struts encompassed by the epiphyseal ring occurs with MN mice (Figure 4 and Table 6). Also, the MN mouse exhibited major abnormalities in trabecular anisotropy, connectivity and structural modeling indexes (Table 6). Figure 4 shows these changes in 3 dimensions. Of note, the reduced SMI index confirms the MN mouse trabecular structure is phased towards a more plate like form compared to the rod like structure of wild type mice.

All of the MN bone phenotypic changes were reversed and almost completely corrected with MNAt mice. MNAt mice did however develop a mineralization defect that did not occur in MN mice but was reminiscent of the defect occurring in the HYP mouse. Specifically, the trabecular osteoid-volume/bone volume (OV/BV) and osteoid width (O.Wi) significantly increased in MNAt mice compared to wild type and MN mice (Table 5). Excessive over expression of ASARM-peptide a known mineralization inhibitor was likely responsible for this abnormality. The hypophosphatemia of MNAt mice compared to the hyperphosphatemia of MN mice likely also played a role in the observed hyperosteoidosis.

ASARM-peptide over expression corrects MN-mice cortical bone abnormalities

MN mice femurs developed extensive structural and anatomic defects (Figure 4 and Table 7). An increase in femur length accompanied by a widening of the cortical ring occurred. Both the endosteal and periosteal circumferences increased along with an increase in marrow volume (Figure 4 and Table 7). The cortical thickness (Ct.Th) however remained normal. Overall these changes resulted in dramatically lengthened and widened femur tube with an unchanged thickness. Although the bone-volume/total-volume (BV/TV) remained normal both the TV and BV increased and the mean bone volume hydroxyapatite content (HAA mg cm^{-3}) decreased significantly relative to wild type (WT) femurs (Figure 4 and Table 7). This resulted in a marked increase in MN-mice moment of inertia (MOI) and inferred bone strength. Except for the HAA, A dramatic reversal in all these metrics occurred with MNAt mice. Indeed, an overcompensated change in the MNAT-mice Ct.Th and MOI occurred with both decreased relative to WT-mice. Also, like HYP mice, a decrease in MNAt bone-surface/bone-volume (BS/BV) relative to WT-mice occurred (Figure 4 and Table 7).

MN bone defects are worsened with age and reversed by ASARM-peptide over expression

Dual Energy X-Ray Absorptiometric (DEXA) measurements revealed striking and accelerated changes in femur bone mineral density (BMD) and bone mineral content (BMC) over time with MN and MNAt mice (Figure 3 (E & F)). Similar changes occurred with total, vertebral and humeral BMD/BMC measurements (data not shown). Relative to WT-type mice, the BMD and BMC for MN-mice increased progressively and for MNAt-mice these metrics decreased progressively (Figure 3 (E & F)). For young mice the BMD and BMC measurements between WT, MN and MNAt mice were similar. In contrast, as mice aged the differences between WT, MN and MNAt mice were striking and significant. Thus, complete loss of MEPE (MN-mice) resulted in an increase in bone mineral; over expression of ASARM-peptide (MNAT-mice) reversed and over compensated this phenotype causing a loss of bone mineral over time.

Author Manuscript Author Manuscript Author Manuscript Author Manuscript

Consistent with the increased bone mass, a decreased serum sclerostin, decreased SOST (sclerostin gene) bone-expression and increased active β-catenin occurred with MN-mice (Figure 5; Tables 1 & 2). Interestingly, unlike the decrease in bone SOST expression, MN-mice renal SOST expression was increased (Table 3). Also unexpectedly, given the reduced bone mass, the circulating sclerostin of MNAt-mice was the same as MN mice, reduced (Table 1). However, this contrasted with MnAt SOST mRNA bone-expression that increased (Table 2). Relative to MN-mice, MNAt bone active β-catenin was increased further. Consistent with the mineralization defects, an increase in HYP-mice sclerostin occurred as reported previously (33,34).

Discussion

Previous studies have reported the changes in the MN-mice bone phenotype but not renal phosphate handling or function (18). For the first time we describe a more detailed analysis of the bone and renal changes occurring with age. Also, the protein regions of MEPE and thus inferred processing responsible for preserving a normal bone mineral phenotype are unknown. We hypothesized a conserved C-terminal region of MEPE shared with other SIBLINGs (for example DMP1, DSPP, Osteopontin, Statherin and BSP) and called the ASARM-motif plays a role. To test our theory we over expressed ASARM-peptide in MN mice (MNAt) and compared the bone and renal phenotypic changes to MN, wild-type (WT) and HYP mice. An increase in ASARM-peptides occurs with PHEX-defective HYP-mice and this causes the mineralization defects (9,11,13,15,34,53). Our study shows the ASARM-motif of MEPE when released as a free ASARM-peptide plays a major role in preserving: 1) normal trabecular structure; 2) normal bone mass; 3) anatomically normal femur proportions; 4) normal renal phosphate handling; and 5) normal renal filtration. The N-terminal region of MEPE may also influence purine metabolism and uric acid (UA) production. This is of interest since human studies show high levels of uric acid are associated positively with bone mass (50-52). Although, computer tomographic measurement of moments of inertia (MOI) indicates the transgenic expression of ASARM-peptide in MN-mice reverses the progressive increase in MN-mice bone-strength; MOI is an indirect computational calculation. Thus, a confirmation of the bone-strength changes in MN-mice needs direct experimental testing using three point bending tests. ASARM-peptides effects in all these areas are progressively more important as animals' age.

Loss of bone mineral and trabecular integrity with age is of major concern for elderly patients with osteoporosis (1,2). Another associated feature of aging is the decline in glomerular filtration rate (GFR) (2). Whether the decline in GFR is normal to aging or signals underlying diseases that attend senescence is unknown (54-56). Serum MEPE levels correlate with age, PTH, serum phosphate, total hip BMD and femur neck BMD (27). Also, extensive studies show strong genome wide association (GWA) for MEPE, BMD and osteoporosis (19-24,26,57,58). Thus, there is compelling evidence that MEPE and MEPE processing plays a role in preserving bone quality and mineral renal homeostasis with aging. For the first time we show that MN mice not only have increased bone mass and trabecular content with aging but also an increased creatinine-clearance. The increased creatinine-clearance suggests an increased glomerular filtration rate (GFR) and a *possible* hyperfiltration defect. Importantly, although creatinine-clearance is one of the most common

Author Manuscript Author Manuscript Author Manuscript Author Manuscript

methods used to estimate GFR, we cannot discount the possibility that an increased renal secretion of creatinine and not GFR occurs in MN mice. Specifically, in C57BL/6 mice there is a significant secretory contribution to creatinine excretion mediated through the organic anion transport system (49). Thus, further studies are needed to confirm whether MN mice show a hyperfiltration abnormality or an increased renal excretion of creatinine. Intriguingly, the MN mice also showed increased expression of renal VEGF (Table 3). The increased VEGF expression is consistent with the MN-mice hyperfiltration hypothesis. This is because of the inferred VEGF altered vascular supply and thus renal plasma blood flow. Consistent with this we previously reported altered renal vasculogenesis in transgenic mice over expressing full-length MEPE (14). Of note, MN-mice fasting glucose levels were normal suggesting the apparent hyperfiltration was not because of incipient diabetes. The increased creatinine-clearance accompanied a worsening hyperphosphatemia with increased renal Na^+-dependent phosphate cotransporters (NPT2A and C) expression, increased $1,25(OH)_2$ D_3 and reduced FGF23. Unexpectedly, an increase in the fractional excretion of phosphate (FEP) occurred with MN-mice despite the hyperphosphatemia. This suggests an abnormality in the MN-mice intestinal-bone-renal phosphate axis caused the hyperphosphatemia. Confirmation of the intestinal-phosphate link needs further studies. Agreeing with previous work, the increased bone mass in MN-mice was because of increased numbers and activities of osteoblasts (Ob.N/BS) and increased bone formation rate (BFR/TV) (18). We found no evidence for a change in osteoclast activity or reduced bone-resorption in MN-mice. The progressive temporal change in MN-mice bone-mass is shown by the dramatic increases in both BMC and BMD over time (DEXA analysis). Thus, studies on younger MN-mice will likely miss or underestimate the phenotypic cortical and trabecular bone abnormalities that accumulate with age (59). Also, consistent with the MN-mice bone phenotype we found reduced serum sclerostin levels, reduced bone sclerostin expression (SOST) and increased bone active β-catenin. Intriguingly, in contrast to the MN-mice increased bone SOST-expression, MN-mice kidneys had decreased SOST expression levels.

In support of MEPE processing, our data shows transgenic over expression of ASARM-peptide in MN-mice (MNAt) reverses the increased bone mass, abnormal trabecular content, hyperphosphatemia and renal creatinine-clearance seen in the MN-mice. A normalization of MNAt osteoblast numbers (Ob.N/BS) and bone formation rate (BFR/TV) chiefly engineered the correction in MNAt-mice bone-mass. Also, MNAt-mice bone resorption remained normal. In contrast to MN-mice, MNAt mice showed trabecular hypomineralization abnormalities. The constitutively increased MNAt-mice ASARM-peptide level, increased FGF23 and hypophosphatemia was likely responsible for this. Consistent with this are the high levels of ASARM-peptides in HYP-mice and the known role ASARM-peptides play in X-linked and autosomal rickets defects (4,9,11,13,15,33,34,53). Of note, the MNAt hypomineralization defect and hypophosphatemia was milder than the HYP-mice defect. This was likely because MNAt-mice unlike HYP-mice have a normal PHEX gene and can compensate partially for the high ASARM-peptide levels. Remarkably, a decrease in circulating sclerostin occurred with MNAt-mice that was greater than that in MN-mice. Also, this accompanied a major increase in MNAt-mice bone active β-catenin that exceeded the increase found with MN-mice. This finding shows the underlying complexity of

Author Manuscript Author Manuscript Author Manuscript Author Manuscript

sclerostin and Wnt/β-catenin signaling in modulating bone mass, structure and mineralization (12,33,34,60). A recent elegant paper that studied the changes in mineral content and bone mass in sclerostin null and sclerostin transgenic mice also supports this notion (60). The authors used a sophisticated approach to show suppressed mineralization kinetics occur in sclerostin deficient mice ($SOST^{-/-}$) with high bone mass. The high rates of bone formation with continuing bone resorption were suggested to be responsible. Both the MN and MNAt mice have low sclerostin and high β-catenin levels but only the MN mice have high bone-mass and increased bone formation. Also, the MN-mice have normal mineralization kinetics and the MNAt-mice display significant hypomineralization. Of note, the MNAt-mice decrease in sclerostin expression was greater than the MN-mice and the active bone β-catenin levels were higher. Thus, consistent with the different osteosclerotic diseases the MN and MNAt-mice for the first time highlight the importance of MEPE and ASARM-peptide processing on bone material properties.

The increased creatinine-clearance and inferred renal hyperfiltration present in MN mice and corrected in MNAt mice is intriguing. Of note, although reduced bone and serum sclerostin occurred with both MN and MNAt mice, renal sclerostin expression was normal in MNAt-mice but increased in MN-mice. Also, a normalization of the MN-mice increased renal VEGF expression occurred with the MNAt-mice. Urine BUN and food intake was normal for both mice with no evidence for proteinuria. The increased renal but not bone VEGF in MN-mice implies a change in kidney vasculature and thus renal plasma flow. Also, a recent study showed FGF23 impairs endothelium-dependent vasorelaxation by increasing superoxide levels and reducing nitric oxide bioavailabilty (61). Since a decrease in FGF23 levels occurred with MN-mice this should predispose to vasodilation with increased renal plasma flow; consistent with the apparent or inferred MN-mice hyperfiltration. As discussed earlier, our previous work showed transgenic mice over expressing MEPE (MEPEtg-mice) have increased vascularity, reduced blood-vessel diameters and altered VEGF expression (14). Thus, we conclude the altered renal VEGF/FGF23 expression in MN-mice and inferred vascularity will likely change the renal plasma flow (RPF). The altered RPF and the apparent increased GFR will then predictably change the renal filtration fraction (FF). Depending on afferent or efferent vascular tone and hypo or hypertensive renal outcomes these alterations will likely influence the renal handling of phosphate (FEP). Further, these compound changes may explain why the increased bone-mass, bone-turnover and hyperphosphatemia of the MN-mouse are incongruent with the noted increased FEP. Also, although not measured, an increase in phosphate intestinal uptake in MN-mice may play a major role in the MN-mice hyperphosphatemia. This notion is consistent with *in situ* intestinal loop studies that show recombinant MEPE inhibits uptake of phosphate in the rat intestinal jejunum (32). Specifically, loss of MEPE in the MN-mice may predispose to increased uptake of dietary phosphate. Thus, with MN-mice the dietary intake of phosphate likely exceeds renal excretion even in the face of an increased FEP. The overcompensation shown in MNAt-mice with hypophosphatemia and correction of the increased creatinine-clearance suggests a major role for ASARM-peptides. Both recombinant MEPE and ASARM-peptides inhibit renal and intestinal phosphate uptake and increase FGF23 expression (8,11,15,31-34,37). Also, the drop in ASARM-peptide levels and reduced FGF23 shown in MN-mice and reversal in MNAt mice is consistent with the ASARM-model (4).

Author Manuscript Author Manuscript Author Manuscript Author Manuscript

Importantly, the use of MNAt mice to test the ASARM-model needs several caveats: (1) MNAt transgenic mice overexpress ASARM-peptides at supra-physiological levels and so the phenotypic overcorrection may reflect this; (2) the high ASARM-peptide levels in MnAt mice could have secondary pathophysiological effects that obfuscate normal physiological responses; and (3) although we expressed ASARM-peptides using an osteoblast specific promoter (col1α-[2.3-kb]) the transcriptional control and temporal expression will likely differ to the nascent MEPE promoter.

In conclusion, this study shows the C-terminal ASARM-motif region of MEPE regulates bone-mass, trabecular content and cancellous structure. Expression of the motif as free ASARM-peptide is enough to correct the bone defects shown in $MEPE^{-/-}$ (MN) mice. The ASARM-peptide is also necessary to fine-tune renal function and to balance dietary phosphate/calcium uptake and renal excretion. The N-terminal part of MEPE may influence purine metabolism and uric acid (UA) production. This is of interest since human studies show high levels of uric acid are associated positively with bone mass (50-52). The importance of this peptide and the bone-renal-gut balance it preserves increases as animals age. Changes in MEPE expression, processing and ASARM-peptide levels may play a key role in osteoporosis, CKD-MBD and age related changes in kidney function.

Supplementary Material

Refer to Web version on PubMed Central for supplementary material.

Acknowledgements

The authors would like to thank Ms. Yan Hong for technical assistance in the preparation and staining of histology slides and samples. Also, we thank the National Institutes of Health (National Institute of Arthritis and Musculoskeletal and Skin Diseases) for grant support to P. S. N. Rowe (Grant 5R01AR051598-10).

References

1. Cauley JA, Chalhoub D, Kassem AM, Fuleihan Gel H. Geographic and ethnic disparities in osteoporotic fractures. Nat Rev Endocrinol. 2014; 10(6):338–51. [PubMed: 24751883]
2. Stompor T, Zablocki M, Lesiow M. Osteoporosis in mineral and bone disorders of chronic kidney disease. Pol Arch Med Wewn. 2013; 123(6):314–20. [PubMed: 23711558]
3. Rowe PS, de Zoysa PA, Dong R, Wang HR, White KE, Econs MJ, Oudet CL. MEPE, a new gene expressed in bone marrow and tumors causing osteomalacia. Genomics. 2000; 67(1):54–68. [PubMed: 10945470]
4. Rowe PS. Regulation of Bone-Renal Mineral and Energy Metabolism: The PHEX, FGF23, DMP1, MEPE ASARM Pathway. Critical reviews in eukaryotic gene expression. 2012; 22(1):61–86. [PubMed: 22339660]
5. Salmon B, Bardet C, Khaddam M, Naji J, Coyac BR, Baroukh B, Letourneur F, Lesieur J, Decup F, Le Denmat D, Nicoletti A, Poliard A, Rowe PS, Huet E, Vital SO, Linglart A, McKee MD, Chaussain C. MEPE-Derived ASARM Peptide Inhibits Odontogenic Differentiation of Dental Pulp Stem Cells and Impairs Mineralization in Tooth Models of X-Linked Hypophosphatemia. PLoS One. 2013; 8(2):e56749. [PubMed: 23451077]
6. Staines KA, Mackenzie NC, Clarkin CE, Zelenchuk L, Rowe PS, MacRae VE, Farquharson C. MEPE is a novel regulator of growth plate cartilage mineralization. Bone. 2012; 51(3):418–30. [PubMed: 22766095]
7. Boskey AL, Chiang P, Fermanis A, Brown J, Taleb H, David V, Rowe PS. MEPE's Diverse Effects on Mineralization. Calcif Tissue Int. 2010; 86(1):42–6. [PubMed: 19998030]

Author Manuscript Author Manuscript Author Manuscript Author Manuscript

8. Rowe PS, Kumagai Y, Gutierrez G, Garrett IR, Blacher R, Rosen D, Cundy J, Navvab S, Chen D, Drezner MK, Quarles LD, Mundy GR. MEPE has the properties of an osteoblastic phosphatonin and minhibin. Bone. 2004; 34(2):303–19. [PubMed: 14962809]

9. Bresler D, Bruder J, Mohnike KL, Fraser D, Rowe PSN. Serum MEPE-ASARM-peptides are elevated in X-linked rickets (HYP): implications for phosphaturia and rickets. J Endocrinol. 2004; 183:R1–9. [PubMed: 15590969]

10. Opsahl Vital S, Gaucher C, Bardet C, Rowe PS, George A, Linglart A, Chaussain C. Tooth dentin defects reflect genetic disorders affecting bone mineralization. Bone. 2012; 50(4):989–97. [PubMed: 22296718]

11. David V, Martin AC, Hedge AM, Drezner MK, Rowe PS. ASARM peptides: PHEX-dependent & independent regulation of serum phosphate. Am J Physiol Renal Physiol. 2011; 300(3):F783–791. [PubMed: 21177780]

12. Atkins GJ, Rowe PS, Lim HP, Welldon KJ, Ormsby R, Wijenayaka AR, Zelenchuk L, Evdokiou A, Findlay DM. Sclerostin is a locally acting regulator of late-osteoblast/pre-osteocyte differentiation and regulates mineralization through a MEPE-ASARM dependent mechanism. J Bone Miner Res. 2011; 26(7):1425–36. [PubMed: 21312267]

13. Boukpessi T, Gaucher C, Leger T, Salmon B, Le Faouder J, Willig C, Rowe PS, Garabedian M, Meilhac O, Chaussain C. Abnormal presence of the matrix extracellular phosphoglycoprotein-derived acidic serine- and aspartate-rich motif peptide in human hypophosphatemic dentin. Am J Pathol. 2010; 177(2):803–12. [PubMed: 20581062]

14. David V, Martin A, Hedge AM, Rowe PS. Matrix extracellular phosphoglycoprotein (MEPE) is a new bone renal hormone and vascularization modulator. Endocrinology. 2009; 150(9):4012–23. [PubMed: 19520780]

15. Martin A, David V, Laurence JS, Schwarz PM, Lafer EM, Hedge AM, Rowe PS. Degradation of MEPE, DMP1, and release of SIBLING ASARM-peptides (minhibins): ASARM-peptide(s) are directly responsible for defective mineralization in HYP. Endocrinology. 2008; 149(4):1757–72. [PubMed: 18162525]

16. Rowe PS, Matsumoto N, Jo OD, Shih RN, Oconnor J, Roudier MP, Bain S, Liu S, Harrison J, Yanagawa N. Correction of the mineralization defect in hyp mice treated with protease inhibitors CA074 and pepstatin. Bone. 2006; 39(4):773–786. [PubMed: 16762607]

17. Rowe PSN, Garrett IR, Schwarz PM, Carnes DL, Lafer EM, Mundy GR, Gutierrez GE. Surface Plasmon Resonance (SPR) confirms MEPE binds to PHEX via the MEPE-ASARM-motif: A model for impaired mineralization in X-linked rickets (HYP). Bone. 2005; 36(1):33–46. [PubMed: 15664000]

18. Gowen LC, Petersen DN, Mansolf AL, Qi H, Stock JL, Tkalcevic GT, Simmons HA, Crawford DT, Chidsey-Frink KL, Ke HZ, McNeish JD, Brown TA. Targeted Disruption of the Osteoblast/Osteocyte Factor 45 Gene (OF45) Results in Increased Bone Formation and Bone Mass. J Biol Chem. 2003; 278(3):1998–2007. [PubMed: 12421822]

19. Zhang L, Choi HJ, Estrada K, Leo PJ, Li J, Pei YF, Zhang Y, Lin Y, Shen H, Liu YZ, Liu Y, Zhao Y, Zhang JG, Tian Q, Wang YP, Han Y, Ran S, Hai R, Zhu XZ, Wu S, Yan H, Liu X, Yang TL, Guo Y, Zhang F, Guo YF, Chen Y, Chen X, Tan L, Zhang L, Deng FY, Deng H, Rivadeneira F, Duncan EL, Lee JY, Han BG, Cho NH, Nicholson GC, McColskey E, Eastell R, Prince RL, Eisman JA, Jones G, Reid IR, Sambrook PN, Dennison EM, Danoy P, Yerges-Armstrong LM, Streeten EA, Hu T, Xiang S, Papasian CJ, Brown MA, Shin CS, Uitterlinden AG, Deng HW. Multi-stage genome-wide association meta-analyses identified two new loci for bone mineral density. Hum Mol Genet. 2014; 23(7):1923–33. [PubMed: 24249740]

20. Hsu YH, Kiel DP. Clinical review: Genome-wide association studies of skeletal phenotypes: what we have learned and where we are headed. J Clin Endocrinol Metab. 2012; 97(10):E1958–77. [PubMed: 22965941]

21. Zmuda JM, Yerges-Armstrong LM, Moffett SP, Klei L, Kammerer CM, Roeder K, Cauley JA, Kuipers A, Ensrud KE, Nestlerode CS, Hoffman AR, Lewis CE, Lang TF, Barrett-Connor E, Ferrell RE, Orwoll ES. Genetic analysis of vertebral trabecular bone density and cross-sectional area in older men. Osteoporosis international. 2011; 22(4):1079–90. [PubMed: 21153022]

22. Jemtland R, Holden M, Reppe S, Olstad OK, Reinholt FP, Gautvik VT, Refvem H, Frigessi A, Houston B, Gautvik KM. Molecular disease map of bone characterizing the postmenopausal

Author Manuscript Author Manuscript Author Manuscript Author Manuscript

osteoporosis phenotype. Journal of bone and mineral research. 2011; 26(8):1793–801. [PubMed: 21452281]

23. Styrkarsdottir U, Halldorsson BV, Gudbjartsson DF, Tang NL, Koh JM, Xiao SM, Kwok TC, Kim GS, Chan JC, Cherny S, Lee SH, Kwok A, Ho S, Gretarsdottir S, Kostic JP, Palsson ST, Sigurdsson G, Sham PC, Kim BJ, Kung AW, Kim SY, Woo J, Leung PC, Kong A, Thorsteinsdottir U, Stefansson K. European bone mineral density loci are also associated with BMD in East-Asian populations. PLoS One. 2010; 5(10):e13217. [PubMed: 20949110]
24. Alam I, Padgett LR, Ichikawa S, Alkhouli M, Koller DL, Lai D, Peacock M, Xuei X, Foroud T, Edenberg HJ, Econs MJ. Sibling Family Genes And Bone Mineral Density: Association And Allele-Specific Expression In Humans. Bone. 2014; 64:166–72. [PubMed: 24747200]
25. Reijnders CM, van Essen HW, van Rens BT, van Beek JH, Ylstra B, Blankenstein MA, Lips P, Bravenboer N. Increased Expression of Matrix Extracellular Phosphoglycoprotein (MEPE) in Cortical Bone of the Rat Tibia after Mechanical Loading: Identification by Oligonucleotide Microarray. PLoS One. 2013; 8(11):e79672. [PubMed: 24255709]
26. Estrada K, Styrkarsdottir U, Evangelou E, Hsu YH, Duncan EL, Ntzani EE, Oei L, Albagha OM, Amin N, Kemp JP, Koller DL, Li G, Liu CT, Minster RL, Moayyeri A, Vandenput L, Willner D, Xiao SM, Yerges-Armstrong LM, Zheng HF, Alonso N, Eriksson J, Kammerer CM, Kaptoge SK, Leo PJ, Thorleifsson G, Wilson SG, Wilson JF, Aalto V, Alen M, Aragaki AK, Aspelund T, Center JR, Dailiana Z, Duggan DJ, Garcia M, Garcia-Giralt N, Giroux S, Hallmans G, Hocking LJ, Husted LB, Jameson KA, Khusainova R, Kim GS, Kooperberg C, Koromila T, Kruk M, Laaksonen M, Lacroix AZ, Lee SH, Leung PC, Lewis JR, Masi L, Mencej-Bedrac S, Nguyen TV, Nogues X, Patel MS, Prezelj J, Rose LM, Scollen S, Siggeirsdottir K, Smith AV, Svensson O, Trompet S, Trummer O, van Schoor NM, Woo J, Zhu K, Balcells S, Brandi ML, Buckley BM, Cheng S, Christiansen C, Cooper C, Dedoussis G, Ford I, Frost M, Goltzman D, Gonzalez-Macias J, Kahonen M, Karlsson M, Khusnutdinova E, Koh JM, Kollia P, Langdahl BL, Leslie WD, Lips P, Ljunggren O, Lorenc RS, Marc J, Mellstrom D, Obermayer-Pietsch B, Olmos JM, Pettersson-Kymmer U, Reid DM, Riancho JA, Ridker PM, Rousseau F, Lagboom PE, Tang NL, et al. Genome-wide meta-analysis identifies 56 bone mineral density loci and reveals 14 loci associated with risk of fracture. Nature genetics. 2012; 44(5):491–501. [PubMed: 22504420]
27. Jain A, Fedarko NS, Collins MT, Gelman R, Ankrom MA, Tayback M, Fisher LW. Serum levels of matrix extracellular phosphoglycoprotein (MEPE) in normal humans correlate with serum phosphorus, parathyroid hormone and bone mineral density. J Clin Endocrinol Metab. 2004; 89(8):4158–61. [PubMed: 15292364]
28. Rowe PS. The chicken or the egg: PHEX, FGF23 and SIBLINGs unscrambled. Cell Biochem Funct. 2012; 30(5):355–75. [PubMed: 22573484]
29. Addison W, Masica D, Gray J, McKee MD. Phosphorylation-Dependent Inhibition of Mineralization by Osteopontin ASARM Peptides is Regulated by PHEX Cleavage. J Bone Miner Res. 2009; 25(4):695–705. [PubMed: 19775205]
30. Addison W, Nakano Y, Loisel T, Crine P, McKee M. MEPE-ASARM Peptides Control Extracellular Matrix Mineralization by Binding to Hydroxyapatite - An Inhibition Regulated by PHEX Cleavage of ASARM. J Bone Miner Res. 2008; 23(10):1638–49. [PubMed: 18597632]
31. Dobbie H, Unwin RJ, Faria NJ, Shirley DG. Matrix extracellular phosphoglycoprotein causes phosphaturia in rats by inhibiting tubular phosphate reabsorption. Nephrol Dial Transplant. 2008; 23(2):730–3. [PubMed: 18037620]
32. Marks J, Churchill LJ, Edward SD, Unwin R. The Phosphatonin Matrix Extracellular Phosphoglycoprotein (MEPE) Inhibits Renal Intestinal Phosphate Transport in vivo. J Am Soc Nephrol. 2008; 19(12):2313–20. [PubMed: 19005008]
33. Zelenchuk L, Hedge A, Rowe PS. SPR4-peptide Alters Bone Metabolism of Normal and HYP Mice. Bone. 2015; 72:23–33. [PubMed: 25460577]
34. Zelenchuk LV, Hedge AM, Rowe PS. PHEX Mimetic (SPR4-Peptide) Corrects and Improves HYP and Wild Type Mice Energy-Metabolism. PLoS One. 2014; 9(5):e97326. [PubMed: 24839967]
35. Barros NM, Hoac B, Neves RL, Addison WN, Assis DM, Murshed M, Carmona AK, McKee MD. Proteolytic processing of osteopontin by PHEX and accumulation of osteopontin fragments in Hyp

Author Manuscript Author Manuscript Author Manuscript Author Manuscript

mouse bone, the murine model of X-linked hypophosphatemia. J Bone Miner Res. 2013; 28(3): 688–99. [PubMed: 22991293]

36. Campos M, Couture C, Hirata IY, Juliano MA, Loisel TP, Crine P, Juliano L, Boileau G, Carmona AK. Human recombinant endopeptidase PHEX has a strict S1' specificity for acidic residues and cleaves peptides derived from fibroblast growth factor-23 and matrix extracellular phosphoglycoprotein. Biochem J. 2003; 373(1):271–9. [PubMed: 12678920]
37. Shirley DG, Faria NJ, Unwin RJ, Dobbie H. Direct micropuncture evidence that matrix extracellular phosphoglycoprotein inhibits proximal tubular phosphate reabsorption. Nephrol Dial Transplant. 2010; 25(10):3191–5. [PubMed: 20472581]
38. Boukpessi T, Septier D, Bagga S, Garabedian M, Goldberg M, Chaussain-Miller C. Dentin alteration of deciduous teeth in human hypophosphatemic rickets. Calcif Tissue Int. 2006; 79(5): 294–300. [PubMed: 17115324]
39. Gaucher C, Boukpessi T, Septier D, Jehan F, Rowe PS, Garabedian M, Goldberg M, Chaussain-Miller C. Dentin noncollagenous matrix proteins in familial hypophosphatemic rickets. Cells Tissues Organs. 2009; 189(1-4):219–23. [PubMed: 18701809]
40. Zhao M, Harris SE, Horn D, Geng Z, Nishimura R, Mundy GR, Chen D. Bone morphogenetic protein receptor signaling is necessary for normal murine postnatal bone formation. J Cell Biol. 2002; 157(6):1049–60. [PubMed: 12058020]
41. Yuan B, Takaiwa M, Clemens TL, Feng JQ, Kumar R, Rowe PS, Xie Y, Drezner MK. Aberrant Phex function in osteoblasts and osteocytes alone underlies murine X-linked hypophosphatemia. J Clin Invest. 2008; 118(2):722–34. [PubMed: 18172553]
42. Bouxsein ML, Boyd SK, Christiansen BA, Guldberg RE, Jepsen KJ, Muller R. Guidelines for assessment of bone microstructure in rodents using micro-computed tomography. J Bone Miner Res. 2010; 25(7):1468–86. [PubMed: 20533309]
43. Parfitt AM, Drezner MK, Glorieux FH, Kanis JA, Malluche H, Meunier PJ, Ott SM, Recker RR. Bone histomorphometry: standardization of nomenclature, symbols, and units. Report of the ASBMR Histomorphometry Nomenclature Committee. J Bone Miner Res. 1987; 2(6):595–610. [PubMed: 3455637]
44. Ott SM. Histomorphometric measurements of bone turnover, mineralization, and volume. Clin J Am Soc Nephrol 3 Suppl. 2008; 3:S151–6.
45. Pfaffl MW. A new mathematical model for relative quantification in real-time RT-PCR. Nucleic Acids Res. 2001; 29(9):e45. [PubMed: 11328886]
46. Azam N, Zhang MY, Wang X, Tenenhouse HS, Portale AA. Disordered regulation of renal 25-hydroxyvitamin D-1alpha-hydroxylase gene expression by phosphorus in X-linked hypophosphatemic (hyp) mice. Endocrinology. 2003; 144(8):3463–8. [PubMed: 12865326]
47. Fujiwara I, Aravindan R, Horst RL, Drezner MK. Abnormal regulation of renal 25-hydroxyvitamin D-1alpha- hydroxylase activity in X-linked hypophosphatemia: a translational or post-translational defect. J Bone Miner Res. 2003; 18(3):434–42. [PubMed: 12619927]
48. Ranch D, Zhang MY, Portale AA, Perwad F. Fibroblast growth factor 23 regulates renal 1,25-dihydroxyvitamin D and phosphate metabolism via the MAP kinase signaling pathway in Hyp mice. Journal of bone and mineral research. 2011; 26(8):1883–90. [PubMed: 21472778]
49. Eisner C, Faulhaber-Walter R, Wang Y, Leelahavanichkul A, Yuen PS, Mizel D, Star RA, Briggs JP, Levine M, Schnermann J. Major contribution of tubular secretion to creatinine clearance in mice. Kidney Int. 2010; 77(6):519–26. [PubMed: 20032962]
50. Makovey J, Macara M, Chen JS, Hayward CS, March L, Seibel MJ, Sambrook PN. Serum uric acid plays a protective role for bone loss in peri- and postmenopausal women: a longitudinal study. Bone. 2013; 52(1):400–6. [PubMed: 23111314]
51. Sritara C, Ongphiphadhanakul B, Chailurkit L, Yamwong S, Ratanachaiwong W, Sritara P. Serum Uric Acid Levels in Relation to Bone-Related Phenotypes in Men and Women. J Clin Densitom. 2012; 16(3):336–40. [PubMed: 22727551]
52. Nabipour I, Sambrook PN, Blyth FM, Janu MR, Waite LM, Naganathan V, Handelsman DJ, Le Couteur DG, Cumming RG, Seibel MJ. Serum uric acid is associated with bone health in older men: a cross-sectional population-based study. J Bone Miner Res. 2011; 26(5):955–64. [PubMed: 21541998]

Author Manuscript Author Manuscript Author Manuscript Author Manuscript

53. Salmon B, Bardet C, Coyac BR, Baroukh B, Naji J, Rowe PS, Opsahl Vital S, Linglart A, McKee MD, Chaussain C. Abnormal osteopontin and matrix extracellular phosphoglycoprotein localization, and odontoblast differentiation, in X-linked hypophosphatemic teeth. Connect Tissue Res. 2014; 55(S1):79–82. [PubMed: 25158186]

54. Glassock RJ. The GFR Decline With Aginig: A sign of Normal Senescence, Not Disease. Nephrology Times. 2009; 2(9):6–8.

55. Lindeman RD, Tobin J, Shock NW. Longitudinal studies on the rate of decline in renal function with age. J Am Geriatr Soc. 1985; 33(4):278–85. [PubMed: 3989190]

56. Rowe JW, Andres R, Tobin JD, Norris AH, Shock NW. The effect of age on creatinine clearance in men: a cross-sectional and longitudinal study. J Gerontol. 1976; 31(2):155–63. [PubMed: 1249404]

57. Park SE, Oh KW, Lee WY, Baek KH, Yoon KH, Son HY, Lee WC, Kang MI. Association of osteoporosis susceptibility genes with bone mineral density and bone metabolism related markers in Koreans: The Chungju Metabolic Disease Cohort (CMC) study. Endocr J. 2014

58. Rivadeneira F, Styrkarsdottir U, Estrada K, Halldorsson BV, Hsu YH, Richards JB, Zillikens MC, Kavvoura FK, Amin N, Aulchenko YS, Cupples LA, Deloukas P, Demissie S, Grundberg E, Hofman A, Kong A, Karasik D, van Meurs JB, Oostra B, Pastinen T, Pols HA, Sigurdsson G, Soranzo N, Thorleifsson G, Thorsteinsdottir U, Williams FM, Wilson SG, Zhou Y, Ralston SH, van Duijn CM, Spector T, Kiel DP, Stefansson K, Ioannidis JP, Uitterlinden AG. Twenty bone-mineral-density loci identified by large-scale meta-analysis of genome-wide association studies. Nat Genet. 2009; 41(11):1199–206. [PubMed: 19801982]

59. Liu S, Brown TA, Zhou J, Xiao ZS, Awad H, Guilak F, Quarles LD. Role of matrix extracellular phosphoglycoprotein in the pathogenesis of X-linked hypophosphatemia. J Am Soc Nephrol. 2005; 16(6):1645–53. [PubMed: 15843468]

60. Hassler N, Roschger A, Gamsjaeger S, Kramer I, Lueger S, van Lierop A, Roschger P, Klaushofer K, Paschalis EP, Kneissel M, Papapoulos S. Sclerostin Deficiency Is Linked to Altered Bone Composition. J Bone Miner Res. 2014

61. Silswal N, Touchberry CD, Daniel DR, McCarthy DL, Zhang S, Andresen J, Stubbs JR, Wacker MJ. FGF23 directly impairs endothelium-dependent vasorelaxation by increasing superoxide levels and reducing nitric oxide bioavailability. Am J Physiol Endocrinol Metab. 2014; 307(5):E426–36. [PubMed: 25053401]

Author Manuscript Author Manuscript Author Manuscript Author Manuscript

Highlights

- MEPE$^{-/-}$ mice (MN) develop increased bone mass, hyperphosphatemia and creatinine-clearance.
- Transgenic over expression of MEPE C-terminal ASARM-motif corrects MN-mice abnormalities.
- The MEPE ASARM-motif regulates bone mass and renal function as mice age.
- The N-terminal region of MEPE may influence purine and uric acid metabolism.
- The ASARM-motif could be a drug target for osteoporosis.

Author Manuscript Author Manuscript Author Manuscript Author Manuscript

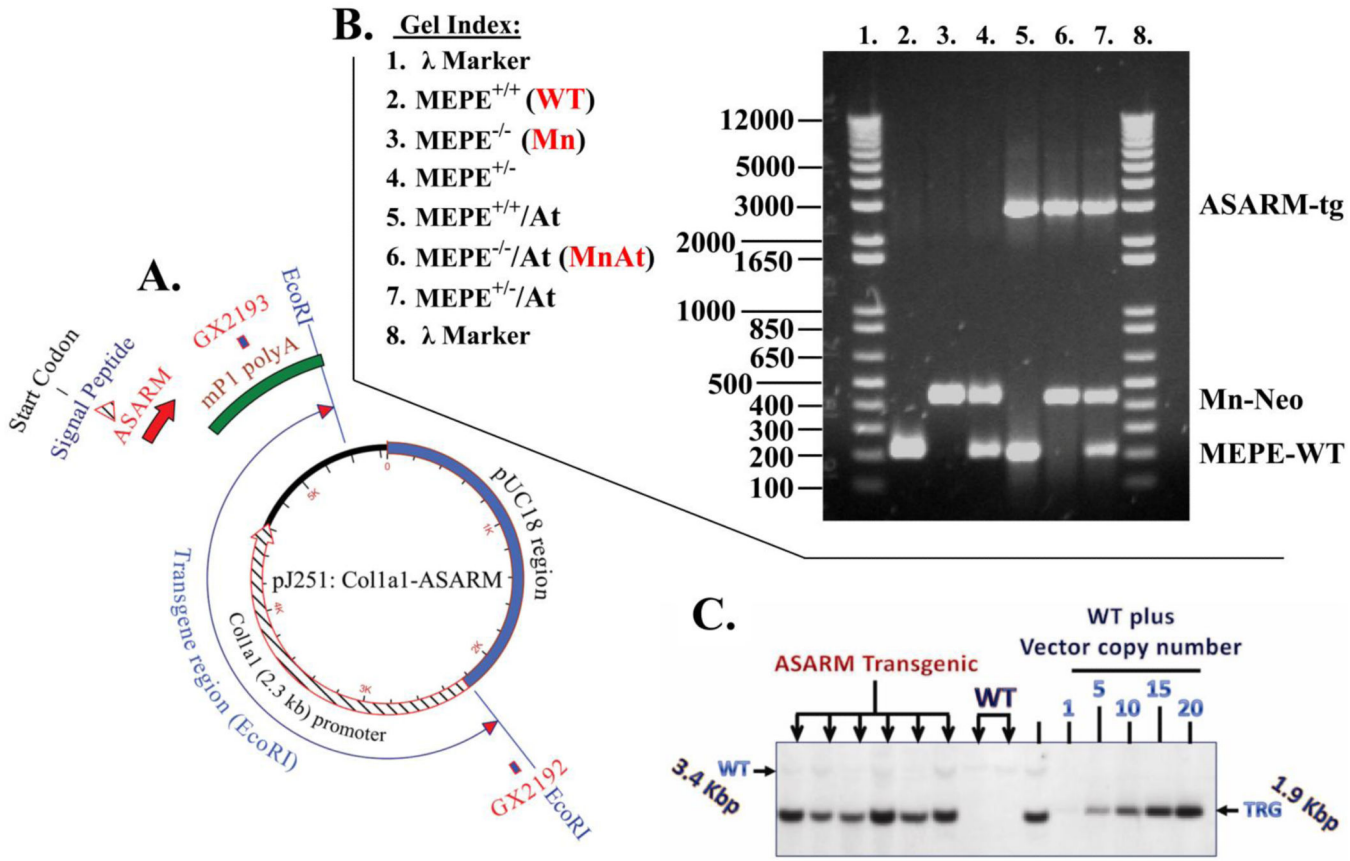

Figure 1.

Illustration and gels showing the construct and protocols for screening mutant mice; **(A)** Vector diagram showing the pJ251-murine-ASARM cloning vehicle with 2.3 kb col1α1 promoter used to generate ASARM-transgenic mice (for complete nucleic acid and protein sequence see supplementary Figures S1 and S2); **(B)** Representative agarose gel that shows the resolved PCR amplified products from wild type (WT) and mutant genomic DNA (see methods for the primers used and Figure S2 for complete sequence). Briefly, a unique MN-mice neo cassette of 430 bp was amplified with NEO50F and NEO430R primers. The WT MEPE$^{+/+}$ band (MEPE-WT) was amplified with MEPEWTF and MEPEWTR primers (215 bp) and the murine ASARM transgenic band (ASARM-tg) was amplified with primers GX2192 and GX2193 (2891 bp). The position of primers GX2192 and GX2193 are shown in Figure 1A and entire vector sequence is shown in Figures S1 and S2; and **(C)** BamHI & BglI Southern genomic DNA blot showing MEPE-transgene integration. For estimation of copy number WT genomic DNA was spiked with 1 to 20 equivalent copies of MEPE-TRG vector. The southern blot was screened with probe labelled and amplified from the vector shown in Figure 1A using primers mep2199 and mep2200 (458 bp) (see methods section for detailed description). The six separate mice shown in Figure 1C are from progeny derived from the same transgenic line selected from a breeder pair with the highest level of serum ASARM-peptides. All subsequent experiments were carried out using descendants from the original breeder C57B/L6 line as described in our previous publication that discussed the characterization and construction of a MEPE transgenic (MEPE-TRG) mouse (14). The

Author Manuscript Author Manuscript Author Manuscript Author Manuscript

transgene copy number correlated positively with circulating levels of ASARM-peptides (r^2=0.8636 and p(two tailed)=0.0073; 95% confidence interval 0.4789 to 0.9924; *Pearson correlation*).

Author Manuscript Author Manuscript Author Manuscript Author Manuscript

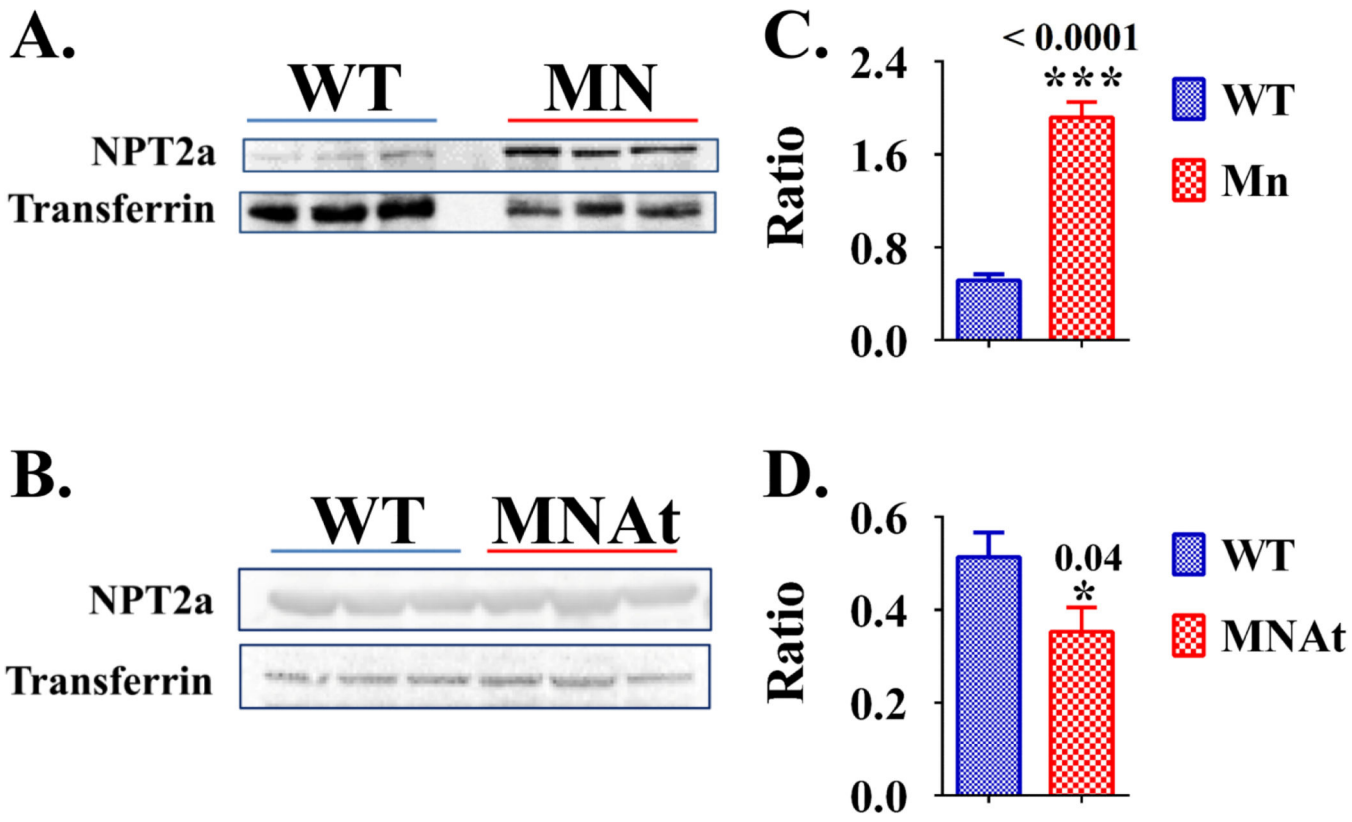

Figure 2.

Whole kidney protein expression of Na dependent phosphate co-transporter NPT2A (Slc34a1) is increased in MN-mice and decreased in MNAt-mice relative to WT-mice: **(A)** western blot protein analysis for NPT2A (Slc34a1) expression for *WT-mice versus MN-mice*; and **(B)** western blot protein analysis for NPT2A (Slc34a1) expression for *WT-mice versus MNAt-mice*; **(C)** corresponding pixel fluorescence analysis of western blot presented as a histogram for *WT-mice versus MN-mice*; and **(D)** corresponding pixel fluorescence analysis of western blot presented as a histogram for *WT-mice versus MNAt-mice*. Male mice (N=6) were sacrificed at age 5.4 months and protein prepared from whole kidneys snap frozen in liquid nitrogen, see methods and previous work (33,34). Results are significant (* = $p<0.05$; student t-test) unless indicated by NS. See Table 3 for corresponding mRNA expression for sodium-dependent phosphate co-transporters NPT2A (Slc34a1) and also NPT2c (Slc34a3). ***Index***: **NPT2a** = Sodium-dependent phosphate co-transporter (Slc34a1); **WT** = Wild type-mice; **MN** = $MEPE^{-/-}$ mice; **MNAt** = $MEPE^{-/-}$/ASARM transgenic mice; * < $P<0.05$; *** < $P<0.0001$.

Author Manuscript Author Manuscript Author Manuscript Author Manuscript

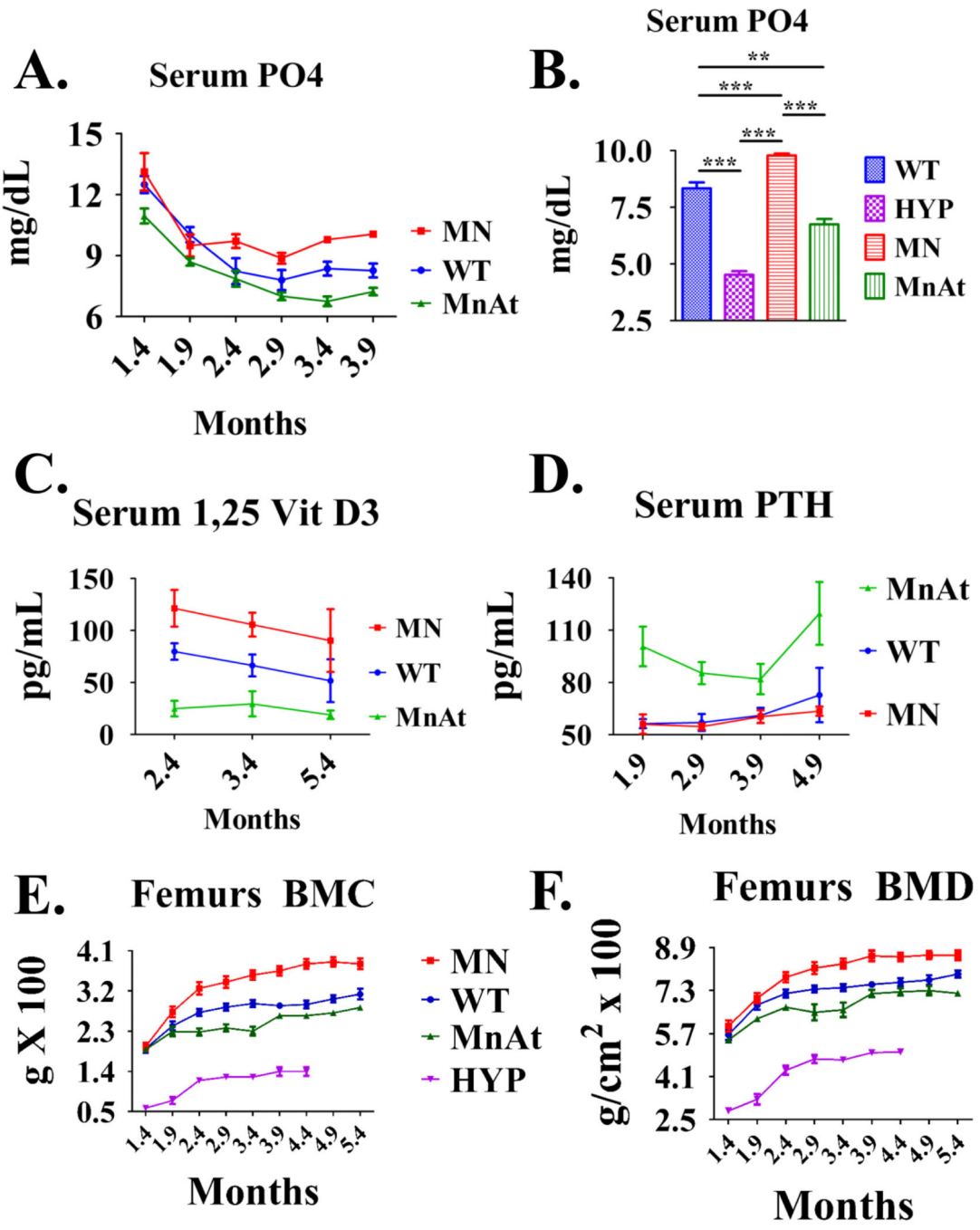

Figure 3.

Temporal changes in serum chemistry **(A, C, D)**, Bone Mineral Content (BMC) **(E)** and Bone Mineral Density (BMD) **(F)**. BMD and BMC (E and F) were measured by Dual Energy X-ray Absorptiometry (DEXA) using Lunar PIXImus as described in methods (N = 6; male mice). Terminal measurements for serum PO4 are illustrated graphically in **(B),** see also Figure 2A and Table 1. A one-way Analysis of variance (*one-way-ANOVA*) followed by a post hoc *Tukey's multi-comparison* test was used to analyze the data in the histogram **(B)** and the following refer to the levels of significance: ** (P=0.001), *** (P< 0.0008); and

Author Manuscript Author Manuscript Author Manuscript Author Manuscript

* (P = 0.01). For temporal changes in serum PO4 **(A)**, a two-way analysis of variance (*2-way-ANOVA*) revealed a highly significant phenotype effect (P<0.0001) and time effect (P<0.0001) with no significant interaction (P=0.4465). For temporal changes in serum 1,25 Vitamin D3 **(C)**, *two-way-ANOVA* analysis revealed a highly significant phenotype effect (P<0.0002). Both time effects (P<0.3819) and interaction (P=0.9702) were not significant. For temporal changes in serum PTH **(D)**, *two-way-ANOVA* analysis revealed a significant phenotype effect (P<0.036) for MNAt mice versus WT and MN mice (P<0.3819) with no significant interaction (P=0.9702). Also, there was no significant difference between WT and MN mice. For temporal changes in BMC **(E)**, *two-way-ANOVA* analysis revealed a highly significant phenotype effect (P<0.0001), time effect (P<0.0001) and significant interaction (P=0.0001). For temporal changes in BMD **(F)**, *two-way-ANOVA* analysis revealed a highly significant phenotype effect (P<0.0001) and time effect (P<0.0001) with no significant interaction (P=0.0641). **Index:** Wild type-mice = WT; $MEPE^{-/-}$ mice = MN; $MEPE^{-/-}$/ASARM transgenic mice = MNAt; and X-linked hypophosphatemic rickets mice = HYP.

Author Manuscript Author Manuscript Author Manuscript Author Manuscript

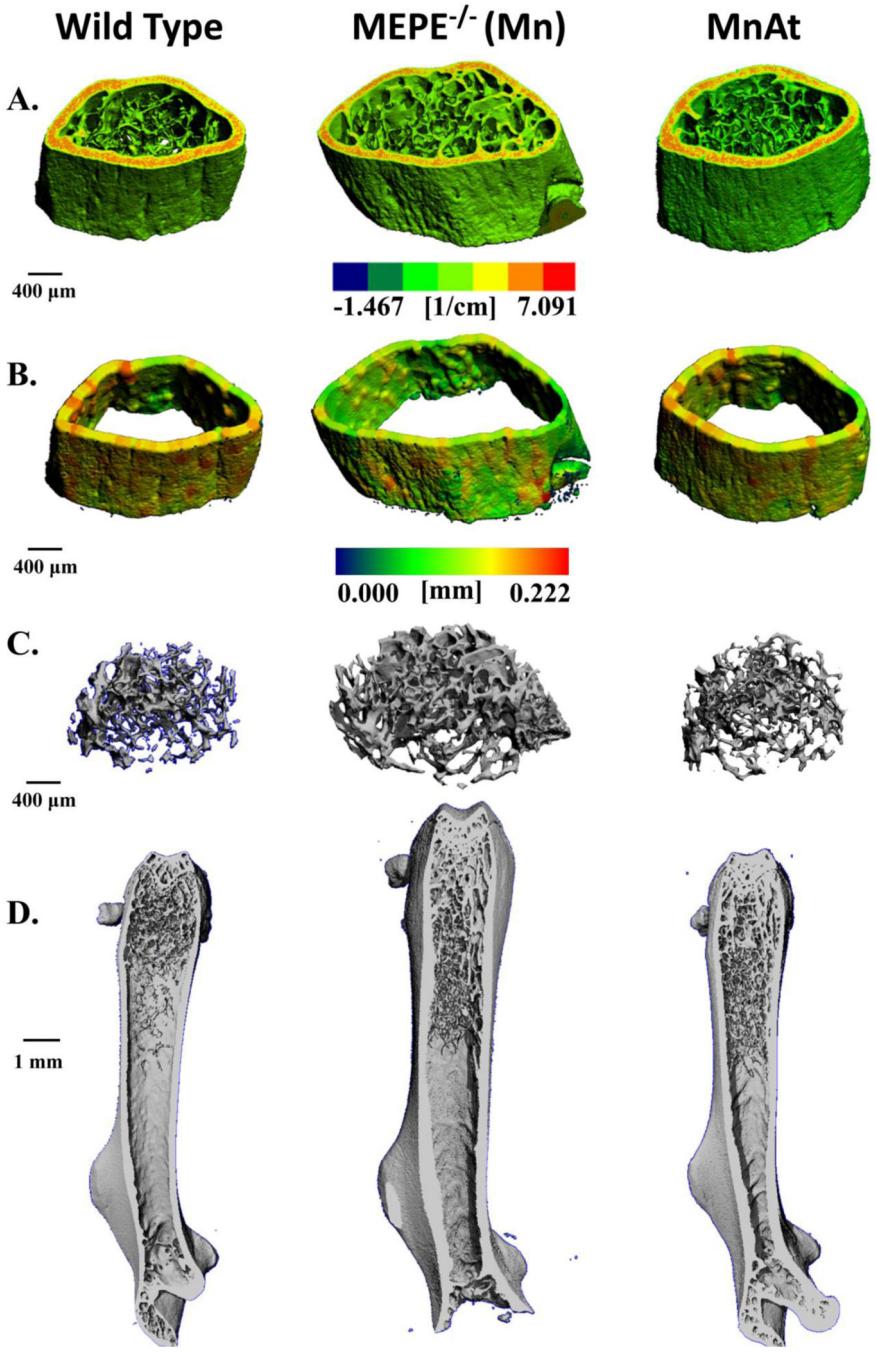

Figure 4.

Bone (femur, epiphyseal cancellous bone) quantitative micro computed tomography (µCT) analysis and 3D colorimetric comparisons for wild type and mutant mice. Over expression of ASARM-peptide in Mn mice (MnAt) rescues the Mn bone phenotype: (**A**) Cross section of femur epiphysis with cortical envelope and cancellous bone. The relative mineral densities are represented by a color scale defined in the figure and in the 3D sections; (**B**) Cross section of femur epiphysis cortical envelope with trabecular cancellous bone removed. The relative modular thickness is represented by a color scale defined in the figure and in

Author Manuscript Author Manuscript Author Manuscript Author Manuscript

the 3D sections; (**C**) Cross section of femur epiphysis trabecular cancellous bone with cortical envelope removed; and (**C**) Cross section of whole femur. The image scale for sections A, B, C and D are shown by bar scales (left hand side).

Author Manuscript Author Manuscript Author Manuscript Author Manuscript

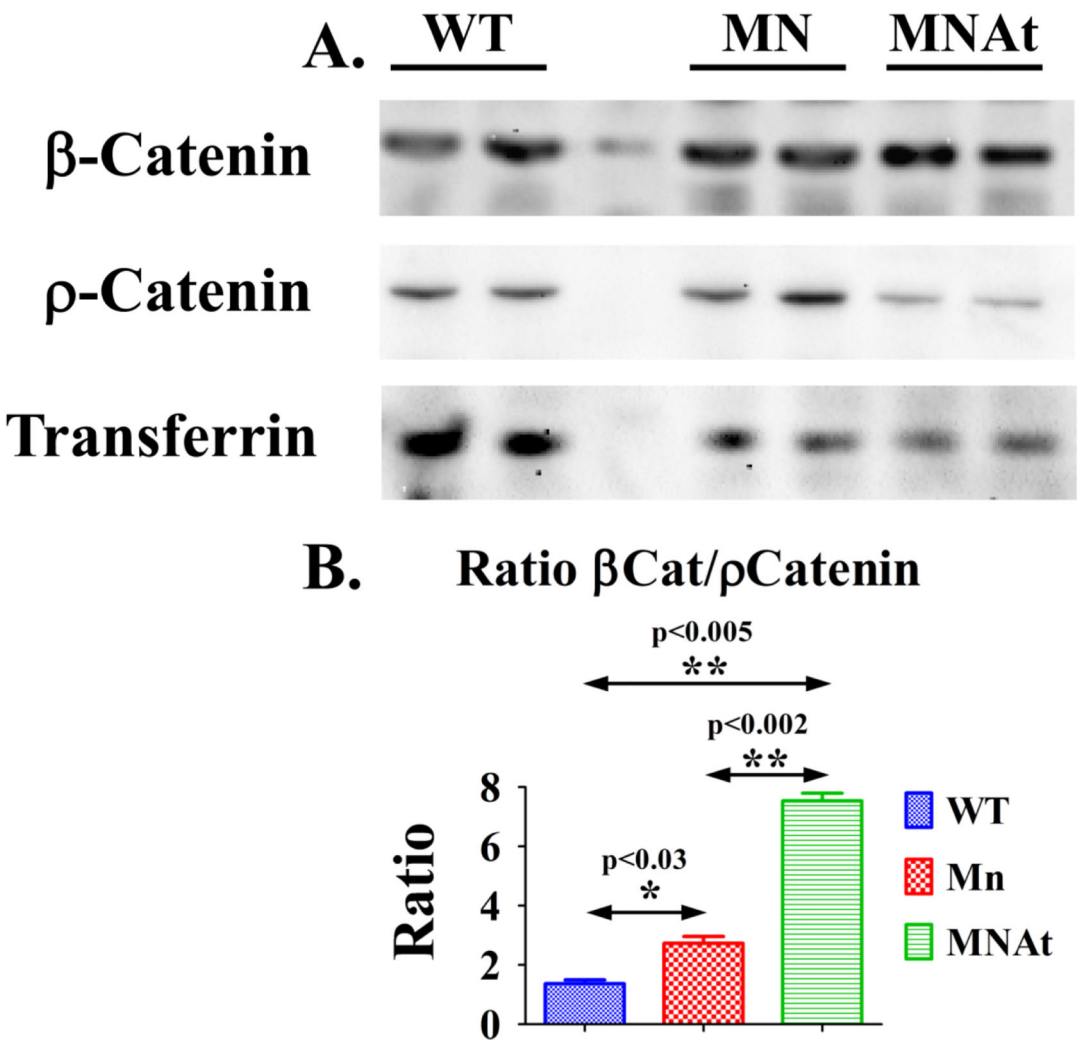

Figure 5.

Active β-Catenin levels are increased in MN and MNAt mice along with changes in static and dynamic cancellous bone histomorphometry; **(A)** Representative western blot of protein lysates prepared from femurs depleted of bone marrow and frozen in liquid nitrogen were screened with anti-β-catenin (β-catenin) and anti-phosphorylated β-catenin (ρ-catenin) and anti-transferrin antibodies as described in methods and published previously (11,14,15,33,34). Male mice (5.4 months; N=6) were fasted for 16 hours and housed singly in metabolic cages (water ad libitum). Also see Table S1 for antibody sources; **(B)** Transferrin was used as an internal control for chemiluminescent pixel density calculations (BioRad Qty1 software and FluorS MaX Imaging). One way Anova and Tukey's Post Test was used to calculate statistical significance (P<0.01* and P<0.001**). ***Index:*** wild type mice (WT), MEPE$^{-/-}$ mice (MN), MEPE$^{-/-}$/ASARM-transgenic mice (MNAt) and X-linked hypophosphatemic mice (HYP).

Author Manuscript Author Manuscript Author Manuscript Author Manuscript

Table 1

Serum chemistry results & comparisons for wild type & mutant mice.

	Serum Values							
Serum Markers	**WT (n=9)**		**MN (n=6)**	**I**	**MNAt (n=6)**		**HYP (n=9)**	
	*****		***§***	**I**	***ρ***		***#***	
Phosphorus mg/dL	8.3 ± 0.22	*§ρ#*	9.8 ± 0.08	**ρ#*	6.7 ± 0.23	**§#*	4.5 ± 0.16	**§ρ*
Calcium mg/dL	8.4 ± 0.24		9.3 ± 0..70		8.9 ± 0.31		8.7 ± 0.30	
1,25(OH)$_2$ pg/mL	66.4 ± 10.5	*§ρ#*	105.1± 11.4	**ρ*	29.5± 12.1	**§#*	92.4± 6.2	**§ρ*
FGF23 pg/mL	192 ± 11.4	*§ρ#*	136.3 ± 13.9	**ρ#*	301.6 ± 29.2	**§#*	2793.6 ± 185	**§ρ*
PTH pg/mL	72.8 ± 15.6	*ρ#*	63.5 ± 2.7	*ρ#*	119.6 ± 17.8	**§*	173.0 ± 21.3	**§*
Alkaline PhAtase U/L	66.6 ± 6.1	*ρ#*	70.1 ± 11.8	*ρ#*	118.5 ± 2.8	**§*	181.1 ± 31.2	**§*
Sclerostin ng/mL	2.3 ± 0.04	*§ρ#*	1.2 ± 0.30	**ρ#*	0.5 ± 0.01	**§#*	3.4 ± 0.01	**§ρ*
Creatinine mg/dL	0.53 ± 0.02	*ρ#*	0.56 ± 0.04	**ρ#*	0.67 ± 0.02	**§#*	0.34 ± 0.03	**§ρ*
MEPE protein ug/mL	3.1 ± 0.17	*§ρ#*	±0.01 ± 0.00	**#*	±0.01 ± 0.00	**#*	7.8 ± 0.36	**§ρ*
ASARM nM	65.0 ± 3.1	*§ρ#*	19.7 ± 6.2	**ρ#*	358.5 ± 4.5	**§#*	277.8 ± 16.3	**§ρ*
Osteocalcin ng/mL	25.49 ± 0.5	*§ρ*	45.8 ± 3.1	**ρ#*	14.5 ± 0.7	**§#*	21.2 ± 2.2	*§ρ*
Adrenaline ng/mL	1.43 ± 0.18	*§ρ#*	2.75 ± 0.14	**ρ#*	2.02 ± 0.13	**§#*	0.74 ± 0.07	**§ρ*
Uric Acid mg/dL	5.6 ± 0.17	*§ρ#*	8.02 ± 0.09	**#*	8.97 ± 0.95	**#*	2.4 ± 0.66	**§ρ*

Serum chemistry results and comparisons for wild type mice (WT), MEPE$^{-/-}$ mice (MN), MEPE$^{-/-}$/ASARM-transgenic mice (MNAt) and X-linked hypophosphatemic mice (HYP): Male mice (N=6) were sacrificed at age 5.4 months and sera plus urine prepared from 16 hour fasted mice housed singly in metabolic cages (water ad libitum). Columns show absolute values with standard error of the means (SEM). Statistical differences between columns were measured by one-way analysis of variance (ANOVA) followed by Tukey's post multi comparison test. Changes that are statistically significant different ($p<0.01$) are denoted by the following superscript codes:

*statistically different to wild type mice (WT)

§statistically different to MEPE$^{-/-}$ mice (MN)

$^{\rho}$statistically different to MEPE$^{-/-}$/ASARM transgenic mice (MNAt) and

$^{\#}$statistically different to X-linked hypophosphatemic rickets mice (HYP).

Author Manuscript Author Manuscript Author Manuscript Author Manuscript

Table 2

Femur gene expression (mRNA) versus wild type

	MN		MNAt		HYP	
Gene	**Mean**	**SEM**	**Mean**	**SEM**	**Mean**	**SEM**
FGF23	−2.5*#$	±0.59	2.8*§#	±0.35	107.7*§$	±3.4
MEPE	NA	?	NA	?	6.2*	±1.41
DMP1	0.9#	±0.21	0.9#	±0.50	5.2*§$	±1.61
SOST	−2.5*#$	±0.52	2.3*§#	±0.20	6.1*§$	±1.80
RANKL	1.1#$	±0.26	3.6*§#	±0.30	7.8*§$	±1.59
GAPDH	0.9#$	±0.17	3.0*§#	±0.30	−6.2*§$	±1.72
PHEX	−3.1*$	±0.71	1.6*§	±0.17	N/A	N/A
SPP1	1.8*	±0.09	1.8*	±0.15	0.9$	±0.07
OPG	−2.1*#$	±0.18	1.5*§	±0.15	1.1	±0.4
RUNX	NS	?	NS	?	ND	?
BGLAP	1.1$	±0.47	2.2*§#	±0.18	1.2$	±0.20
CYPD	NS	?	ND	?	NS	?
ATF4	−3.7*#$	±0.9	2.4*§#	±0.21	−1.8*§$	±0.32
FOXO1	NS	?	NS	?	NS	?
Cyclin D1	0.7#$	±0.11	2.4*§	±0.28	2.2*§	±0.25
MYC	NS	?	NS	?	NS	?
CLOCK	0.8#$	±0.09	1.7*§#	±0.18	−1.4*§$	±0.09
CREB	NS	?	NS	?	NS	?
JUN-C	0.9$	±0.14	2.5*§#	±0.24	1.03$	±0.18
FOS	−1.9*#$	±0.19	3.2*§	±0.32	2.9*§$	±0.22
PER-2	0.9#	±0.11	1.2	±0.15	1.4*§	±0.12
ESP	0.8#$	±0.09	1.6*§	±0.14	2.7*§	±0..81
FAM20C	0.9#$	±0.12	2.1*§	±0.22	2.9*§	±0.30
ENPP1	0.9#$	±0.14	1.9*§	±0.18	2.3*	±0.36
RANK	NS	?	ND	?	NS	?

Bone (femur) mRNA expression profiles as measured by quantitative RT/PCR (qRT-PCR) for wild type and mutant mice. Male mice were sacrificed at 5.4 months and mRNA prepared from bone marrow stromal cell depleted femurs (N=6) as reported previously and in methods (33,34). For qRT-PCR gene analysis fold differences in expression calculated by the Pfaffl method (45) were statistically analyzed for significance using the One Sample t-test and the Wilcoxon Signed rank-test with theoretical means set to 1. The fold changes in expression relative to WT and standard error of the means (SEM) are shown in columns adjacent to the fold expression results. Statistical differences between wild type mice (WT) and columns were measured by one-way analysis of variance (ANOVA) followed by Tukey's post multi comparison test. Changes that are statistically significant different ($p<0.01$) are denoted by the following superscript codes:

Author Manuscript

Author Manuscript

Author Manuscript

Author Manuscript

ρ = statistically different to MEPE$^{-/-}$/ASARM transgenic mice (MNAt) and

*statistically different to wild type mice (WT)

§statistically different to MEPE$^{-/-}$ mice (MN)

$^{\#}$statistically different to X-linked hypophosphatemic rickets mice (HYP): ***Index:*** **FGF23** = Fibroblast Growth Factor 23; **MEPE** = Matrix Extracellular Phosphoglycoprotein with ASARM-motif; **DMP1** = Dentin Matrix Protein 1; **SOST** = Sclerostin; **RANKL** = Receptor Activator for Nuclear Factor κB Ligand; **VEGF** = vascular endothelial growth factor; **GAPDH** = Glyceraldehyde 3-phosphate dehydrogenase; **PHEX** = Phosphate-regulating gene with Homologies to Endopeptidases on the X chromosome; **SPP1** = Secreted phosphoprotein 1 (Osteopontin); **OPG** = Tumor necrosis factor receptor superfamily, member 11b (osteoprotegerin); **RUNX** = Runt-related transcription factor 2 (RUNX2) also known as core-binding factor subunit alpha-1 (CBF-α1); **BGLAP** = osteocalcin or bone γ-carboxyglutamic-acid-containing protein; **CYPD** = Cyclophilin D; **ATF4** = Activating transcription factor 4 (tax-responsive enhancer element B67); **FOXO1** = Forkhead box O1; **CYCLIN D1** = G1/S-specific cyclin-D1; **MYC** = v-myc myelocytomatosis viral oncogene homolog; **CLOCK** = Clock circadian regulator; **CREB** = cAMP response element-binding protein; **JUN-C** = Jun proto-oncogene; **FOS** = FBJ murine osteosarcoma viral oncogene homolog; **PER-2** = Period circadian clock 2; **ESP** = Osteotesticular protein tyrosine (OST-PTP); **FAM20C** = Family with sequence similarity 20, member C Kinase also known as DMP4; **ENPP1** = Ectonucleotide Pyrophosphatase Phosphodiesterase 1; **RANK** = Tumor necrosis factor receptor superfamily, member 11a, NFκB activator; **ND** = Not done; **NS** = Not Significant.

Author Manuscript Author Manuscript Author Manuscript Author Manuscript

Table 3

Whole kidney gene expression (mRNA) versus wild type.

	MN		MNAt		HYP	
Gene	**Mean**	**SEM**	**Mean**	**SEM**	**Mean**	**SEM**
NPT2a	$2.7^{*\#\$}$	±0.26	$2.1^{*\S\#}$	±0.33	$-2.9^{*\S\$}$	±0.25
NPT2c	$2.1^{*\#}$	±0.23	$2.5^{*\#}$	±0.34	$-1.5^{*\S\$}$	±0.06
KLOTHO	$0.9^{\#}$	±0.11	$1.1^{\#}$	±0.28	$-1.4^{*\S\$}$	±0.18
SPP1	$1.1^{\#}$	±0.21	$1.1^{\#}$	±0.11	$-1.3^{*\S\$}$	±0.08
1-α-Ohase	$1.5^{\#\$}$	±0.20	$-7.0^{*\S\#}$	±1.2	$2.4^{*\S\$}$	±0.91
24-Ohase	1.0	±0.32	0.84	±0.22	1.3	±0.28
VEGF	1.9^{*}	±0.17	$1.2^{\#}$	±0.23	3.3^{*}	±0.71
MEPE	NA	-	NA	-	1.2	±0.5
SOST	$1.7^{*\#\$}$	±0.06	$1.0^{\$\#}$	±0.13	$3.2^{*\S\$}$	±0.32

Whole kidney gene expression (mRNA) as measured by quantitative RT/PCR (qRT-PCR) for wild type mice (WT), $MEPE^{-/-}$ mice (MN), $MEPE^{-/-}$/ASARM-transgenic mice (MNAt) and X-linked hypophosphatemic mice (HYP): Male mice (age 5.4 months; N=6) fasted for 16 hours and housed singly in metabolic cages (water ad libitum) were sacrificed and kidneys removed for mRNA extraction. For qRT-PCR gene analysis fold differences in expression calculated by the Pfaffl method (45) were statistically analyzed for significance using the One Sample t-test and the Wilcoxon Signed rank-test with theoretical means set to 1. The fold changes in expression relative to WT and standard error of the means (SEM) are shown in columns adjacent to the fold expression results. Statistical differences between wild type mice (WT) and columns were measured by one-way analysis of variance (ANOVA) followed by Tukey's post multi comparison test. Changes that are statistically significant different ($p<0.01$) are denoted by the following superscript codes:

ρ = statistically different to $MEPE^{-/-}$/ASARM transgenic mice (MNAt) and

*statistically different to wild type mice (WT)

§statistically different to $MEPE^{-/-}$ mice (MN)

$^{\#}$statistically different to X-linked hypophosphatemic rickets mice (HYP): ***Index*: NPT2a** = Sodium-dependent phosphate co-transporter (Slc34a1); **NPT2c** = Sodium-dependent phosphate co-transporter (Slc34a3); **KLOTHO** = type-1 membrane β-glucoronidase; **SPP1** = Secreted phosphoprotein 1 (Osteopontin); **1-α-Ohase** = 25-hydroxyvitamin D3 1-alpha-hydroxylase (CYP27B1); **24-Ohase** = 1,25-hydroxyvitamin D3 24-hydroxylase (CYP24A1); **VEGF** = Vascular Endothelial Growth factor; **MEPE** = Matrix Extracellular Phosphoglycoprotein with ASARM -motif; **SOST** = Sclerostin; **ND** = Not done; **NS** = Not Significant.

Author Manuscript Author Manuscript Author Manuscript Author Manuscript

Table 4

Urine chemistry results & comparisons for wild type & mutant mice.

	Urine Values							
Urine Markers	**WT (n=9)**		**MN (n=6)**		**MNAt (n=6)**		**HYP (n=9)**	
	*		§		ρ		#	
FEP	8.2 ± 0.85	§ρ#	13.5 ± 1.5	*#	15.3 ± 1.4	*#	24.6 ± 3.6	*§ρ
FE-Ca	0.94 ± 0.15	§	0.43 ± 0.07	*ρ#	0.91 ± 0.16	§	0.93 ± 0.03	§
Calcium/Creatinine	0.14 ± 0.016	§	0.08 ± 0.016	*	0.12 ± 0.019		0.18 ± 0.03	
Creatinine Clearance	57.3 ± 6.4	§	96.6 ± 9.0	*ρ#	49.3 ± 8.1	§	58.9 ± 10.5	§
Urine Creatinine (15 hr)	0.34 ± 0.03	§#	0.49 ± 0.06	*ρ#	0.29 ± 0.04	§	0.17 ± 0.02	*§
FE-Uric Acid	6.2 ± 0.5	§#	3.4 ± 0.7	*#	4.4 ± 0.6	*#	17.0 ± 3.4	*§ρ

Urine chemistry results and comparisons for wild type mice (WT), MEPE$^{-/-}$ mice (MN), MEPE$^{-/-}$/ASARM-transgenic mice (MNAt) and X-linked hypophosphatemic mice (HYP): Male mice (N=6) were sacrificed at age 5.4 months and sera plus urine prepared from 16 hour fasted mice housed singly in metabolic cages (water ad libitum). Columns show absolute values with standard error of the means (SEM). Statistical differences between columns were measured by one-way analysis of variance (ANOVA) followed by Tukey's post multi comparison test. Changes that are statistically significant different ($p<0.01$) are denoted by the following superscript codes:

Index: **FEP** = percentage Fractional Excretion of Phosphate (%); **Fe Ca** = percentage Fractional Excretion of Calcium (%); **Calcium/Creatinine** = urinary calcium creatinine ratio ((mg/dL)/(mg/dL)); **Creatinine Clearance** = urinary creatinine clearance (uL/min); **Urine creatinine (15 hr)** = urinary creatinine excretion mg/15 hours; **FE-Uric Acid** = percentage Fractional Excretion of uric acid (%).

*statistically different to wild type mice (WT)

§statistically different to MEPE$^{-/-}$ mice (MN)

$^{\rho}$statistically different to MEPE$^{-/-}$/ASARM transgenic mice (MNAt) and

$^{\#}$statistically different to X-linked hypophosphatemic rickets mice (HYP).

Author Manuscript Author Manuscript Author Manuscript Author Manuscript

Table 5

Femur (trabecular) static/dynamic histomorphometry: Wild type & Mutant Mice.

	Absolute Values							
Femur (Cancellous-bone)	**WT (n=9)**		**MN (n=6)**		**MNAt (n=6)**		**HYP (n=9)**	
	*		§		ρ		#	
BV/TV (%)	20.7 ± 1.5	§#	26.7 ± 1.9	*ρ#	21.4 ± 1.4	§#	2.76 ± 0.49	*§ρ
Tb. Th (um)	51.3 ± 4.1	§	62.3 ± 2.4	*ρ#	46.0 ± 1.6	§	47.5 ± 3.9	§
Tb. Sp (um)	209.4 ± 2.5	§#	163.5 ± 4.5	*ρ#	200.3 ± 6.6	§#	782.7 ± 245.10	*§ρ
Tb.N	3.8 ± 0.07	§#	4.6 ± 0.12	*ρ#	3.9 ± 0.11	§#	1.0 ± 0.20	*§ρ
Oc.S/BS (%)	14.9 ± 3.4	#	20.9 ± 3.2		22.5 ± 4.8		29.2 ± 6.7	*
Oc.N/BS (#/mm)	2.5 ± 0.5	#	2.9 ± 0.32	#	2.3 ± 0.48	#	5.49 ± 0.29	*§ρ
O.Wi (μm)	1.94 ± 0.29	ρ#	1.95 ± 0.32	ρ#	3.1 ± 0.48	*§#	6.1 ± 0.32	*§ρ
OV/BV (%)	0.05 ± 0.03	ρ#	0.08 ± 0.03	ρ#	0.36 ± 0.07	*§#	227.10 ± 28.90	*§ρ
Ob.S (mm)	1.5 ± 0.07	§	2.6 ± 0.28	*ρ	1.4 ± 0.22	§	ND	—
Ob.S/BS (%)	14.8 ± 1.6	§	22.1 ± 2.18	*ρ	15.4 ± 1.82	§	ND	—
Ob.N/BS (#/mm)	11.1 ± 1.8	§	16.7 ± 0.9	*ρ	11.2 ± 0.96	§	ND	—
BFR/TV (per/day)*1000	5.4 ± 0.4	§	7.8 ± 0.66	*ρ	5.8 ± 0.48	§	ND	—
MAR (μm/day)	1.39 ± 0.03	§	1.57 ± 0.05	*ρ	1.27 ± 0.05	§	ND	—

Bone (femur, epiphyseal cancellous bone) histomorphological analysis of histology stained slides (see methods) for wild type mice (WT), MEPE$^{-/-}$ mice (MN), MEPE$^{-/-}$/ASARM-transgenic mice (MNAt) and X-linked hypophosphatemic mice (HYP): Male mice (age 5.4 months; N=6) fasted for 16 hours and housed singly in metabolic cages (water ad libitum) were sacrificed and femurs removed for histology and μCT analyses. Columns show absolute values with standard error of the means (SEM). Statistical differences between columns were measured by one-way analysis of variance (ANOVA) followed by Tukey's post multi comparison test. Changes that are statistically significant different ($p<0.01$) are denoted by the following superscript codes:

Index: **BV/TV (%)** = Bone-volume/total-volume(%); **Tb.Th (μm)** = trabecular thickness (μm); **Tb.Sp(μm)** = trabecular spacing(μm); **Tb.N** = trabecular number (mm^{-1}); **Oc.S/BS (%)** = osteoclast-surface/bone-surface (%); **Oc.N/BS (#/mm)** = osteoclast-number/bone-surface (#/mm); **O.Wi (μm)** = Osteoid Width (%); **OV/BV (%)** = osteoid-volume/bone-volume (%); **Ob.S (mm)** = osteoblast-surface (mm); **Ob.S/BS (%)** = osteoblast-surface/bone-surface (%); **Ob.N/BS (#/mm)** = osteoblast-number/bone-surface (#/mm); **BFR/TV (per/day)*1000** = bone formation rate with tissue volume referent in per day units (μm/day*1000); **MAR (μm/day)** = mineral apposition rate (μm/day).

*statistically different to wild type mice (WT)

§statistically different to MEPE$^{-/-}$ mice (MN)

ρstatistically different to MEPE$^{-/-}$/ASARM transgenic mice (MNAt) and

#statistically different to X-linked hypophosphatemic rickets mice (HYP). Explora-Nova histomorphometric software (F17011 LaRochelle Cedex 1France) was used to analyze the microscopically imaged samples and the guidelines as described by us previously and discussed in methods (14,16,33). The methods and guidelines of Ott 2008 (44) were used to calculate histomorphometric measurements of bone turnover, mineralization and volume. Bone histomorphometric nomenclature, symbols and units were standardized as described by Parfitt et al 1987 (43) with guidelines for assessment from Bouxsein et al 2010 (42).

Author Manuscript Author Manuscript Author Manuscript Author Manuscript

Table 6

Femur (trabecular) quantitative μCT: Wild type & Mutant Mice.

	Absolute Values							
μCT (Cancellous-bone)	**WT (n=9)**		**MN (n=6)**		**MNAt (n=6)**		**HYP (n=9)**	
	*		§		ρ		#	
BV/TV (%) (Trabeculae)	8.1 ± 0.45	§#	15.9 ± 1.5	ρ#	10.3 ± 1.6	*§#	0.6 ± 0.03	*§ρ
BV/TV (%) (cortical ring)	99.3.± 0.025	§	98.7 ± 0.156	*ρ	99.2 ± 0.045	§	ND	—
BS/BV (1/mm) (Trabeculae)	62.0 ± 1.8	ρ	56.4 ± 1.5	*ρ	69.4 ± 2.5	*§	ND	—
Tb.N (1/mm)	2.5 ± 0.07	§#	4.5 ± 0.45	*ρ#	2.9 ± 0.2	§#	1.4 ± 0.03	*§ρ
Tb. Th (μm)	32.3 ± 0.98	§ρ#	35.6 ± 0.097	*ρ#	28.0 ± 1.01	*§#	17.1 ± 0.31	*§ρ
Tb.Sp (mm)	0.37 ± 0.01	§#	0.21 ± 0.02	*ρ#	0.31 ± 0.02	§#	35.1 ± 1.10	*§ρ
Connectivity (1/mm^3)	61.9 ± 3.7	§ρ#	144.6 ± 11.9	*ρ#	102.1 ± 12.9	*§#	38.4 ± 2.5	*§ρ
SMI (1)	2.5 ± 0.06	§	1.3 ± 0.20	*ρ#	2.2 ± 0.09	§#	2.8 ± 0.09	§ρ
Anistropy (1)	1.3 ± 0.03	§#	1.6 ± 0.09	*#	1.4 ± 0.03	#	3.01 ± 0.09	*§ρ
MOI (Cortical Ring) EPI	0.84 ± 0.04	§	1.1 ± 0.08	*ρ#	0.7 ± 0.04	§	0.83 ± 0.03	§
Ct.Th (Cortical Ring) EPI	0.155 ± 0.0016	§ρ#	0.137 ± 0.0029	*#	0.138 ± 0.0025	*#	0.072 ± 0.002	*§ρ

Bone (femur, epiphyseal cancellous bone) quantitative micro computed tomography (uCT) analysis for wild type mice (WT), MEPE$^{-/-}$ mice (MN), MEPE$^{-/-}$/ASARM-transgenic mice (MNAt) and X-linked hypophosphatemic mice (HYP): Male mice (age 5.4 months; N=6) fasted for 16 hours and housed singly in metabolic cages (water ad libitum) were sacrificed and femurs removed for histology and μCT analyses. Columns show absolute values with standard error of the means (SEM). Statistical differences between columns were measured by one-way analysis of variance (ANOVA) followed by Tukey's post multi comparison test. Changes that are statistically significant different ($p<0.01$) are denoted by the following superscript codes:

Index: **BV/TV (%) (Trabeculae)** = trabecular bone-volume/total-volume (%); **BV/TV (%) (cortical-ring)** = bone-volume/total-volume of the cortical ring encompassing the central cancellous (trabecular) core of the epiphysis (%); **BS/BV (1/mm) (Trabeculae)** = bone-surface/total-bone-volume (1/mm); **Tb.N (1/mm)** = trabecular number (1/mm); **Tb.Th (μm)** = trabecular thickness (μm); **Tb.Sp** = trabecular spacing (mm); **Connectivity (1/mm^3)** = number of connected structures calculated by the Euler characteristic (1/mm^3); **SMI (1)** = structural modeling index [1]; **Anisotropy (1)** = anisotropic index of longitudinal/traverse tensile compressive force resistance; **MOI (Cortical Ring) EPI** = moment of inertia of cortical ring encompassing the central cancellous (trabecular) core of the epiphysis; **Ct.Th (Cortical Ring) EPI** = cortical thickness of the cortical ring encompassing the central cancellous (trabecular) core of the epiphysis (mm).

* statistically different to wild type mice (WT)

§ statistically different to MEPE$^{-/-}$ mice (MN)

ρ statistically different to MEPE$^{-/-}$/ASARM transgenic mice (MNAt) and

statistically different to X-linked hypophosphatemic rickets mice (HYP). Micro computed tomography (μCT) using a Scanco μCT 40 system was carried out as described previously and discussed in methods (14,16,33). Bone histomorphometric nomenclature, symbols and units were standardized as described by Parfitt et al 1987 (43) with guidelines for assessment from Bouxsein et al 2010 (42).

Author Manuscript Author Manuscript Author Manuscript Author Manuscript

Table 7

Femur (cortical bone) computed tomography (uCT): Wild type & Mutant Mice

	Absolute Values							
uCT Femur (Cortical-bone)	**WT (n=9)**		**MN (n=6)**		**MNAt (n=6)**		**HYP (n=9)**	
	*		§		ρ		#	
MOI	0.45 ± 0.018	§ #	0.61 ± 0.027	* ρ #	0.39 ± 0.020	§ #	0.29 ± 0.012	* § ρ
BV/TV$_{\delta}$ (%)	99.8 ± 0.00012	ρ #	99.7 ± 0.00032	#	99.6 ± 0.0004	* #	83.3 ± 0.876	* § ρ
BV (mm^3)	1.63 ± 0.04	§ #	1.85 ± 0.05	* ρ #	1.51 ± 0.08	§ #	0.77 ± 0.02	* § ρ
TV$_{\delta}$ (mm^3)	1.64 ± 0.04	§ #	1.86 ± 0.05	* ρ #	1.65 ± 0.07	§ #	0.93 ± 0.04	* § ρ
Ct.Th (mm)	0.205 ± 0.0025	ρ #	0.207 ± 0.0027	ρ #	0.192 ± 0.0038	* § #	0.092 ± 0.0020	* § ρ
BS/BV (1/mm)	10.3 ± 0.10	#	10.8 ± 0.22	#	10.9 ± 0.18	#	21.8 ± 0.37	* § ρ
MV$_{\rho}$ (mm^3) =(Tv$_{\alpha}$-BV)	1.87 ± 0.04	§ #	2.39 ± 0.05	* ρ #	1.93 ± 0.07	§ #	2.04 ± 0.14	* § ρ
Periosteal Circumference	4.91 ± 0.083	§	5.3 ± 0.123	* ρ	4.90 ± 0.079	§	ND	
Endosteal Circumference	3.62 ± 0.082	§	4.13 ± 0.150	* ρ	3.70 ± 0.065	§	ND	
HAA mg cm^{-3} (mean BV)	1384 ± 5.9	#	1349 ± 8.1	#	1356 ± 9.2	#	1168 ± 10.9	* § ρ

Bone (femur, cortical bone) quantitative micro computed tomography (uCT) analysis with results and comparisons for wild type mice (WT), MEPE$^{-/-}$ mice (MN), MEPE$^{-/-}$/ASARM-transgenic mice (MNAt) and X-linked hypophosphatemic mice (HYP): Male mice (age 5.4 months; N=6) fasted for 16 hours and housed singly in metabolic cages (water ad libitum) were sacrificed and femurs removed for histology and μCT analyses. Columns show absolute values with standard error of the means (SEM). Statistical differences between columns were measured by one-way analysis of variance (ANOVA) followed by Tukey's post multi comparison test. Changes that are statistically significant different ($p<0.01$) are denoted by the following superscript codes:

Index: **MOI** = moment of inertia; **BV/TVδ** = bone-volume/total-tissue-volume excluding marrow volume (%); **BV** (mm^3) = bone-volume (mm^3); **TVδ (mm^3)** = total tissue-volume excluding marrow-volume (mm^3); **Ct.Th (mm)** = cortical thickness (mm); **BS/BV (1/mm)** = bone-surface/total-tissue-volume (%); **MV$_{\rho}$ = (mm^3) (TV$_{\alpha}$-BV)** = marrow-volume of defined region of interest (ROI) of central diaphysis (mm^3) where TV$_{\alpha}$ is the total tissue volume including marrow volume and TVδ (mm^3); **Periosteal Circumference** = bone-area (mm); **Endosteal Circumference** = total-area (mm); **HAA mg cm^{-3} (mean BV)** = mean/density of hydroxyapatite.

*statistically different to wild type mice (WT)

§statistically different to MEPE$^{-/-}$ mice (MN)

$^{\rho}$statistically different to MEPE$^{-/-}$/ASARM transgenic mice (MNAt) and

$^{\#}$statistically different to X-linked hypophosphatemic rickets mice (HYP). Micro computed tomography (μCT) using a Scanco μCT 40 system was carried out as described previously and discussed in methods (14,16,33). Bone histomorphometric nomenclature, symbols and units were standardized as described by Parfitt et al 1987 (43) with guidelines for assessment from Bouxsein et al 2010 (42).